GENERATING AN ADAPTIVE AND ROBUST WALKING PATTERN FOR PROSTHETIC ANKLE-FOOT UTILIZING A NONLINEAR AUTOREGRESSIVE NETWORK WITH EXOGENOUS INPUTS

Hamza Al Kouzbary

DISSERTATION SUBMITED IN FULFILMENT OF
THE REQUIRMENTS OF THE DEGREE OF
MASTER OF ENGINEERING SCIENCE

FACULTY OF ENGINEERING

UNIVERSITY OF MALAYA

2021

UNIVERSITY OF MALAYA

ORIGINAL LITERATURE WORK DECLARATION

Name of candidate: Hamza Al Kouzbary

Registration matric No.: 17029207/1

Name of degree: Master of Engineering Science

Title of Dissertation ("this Work"): GENRATING AN ADAPTIVE AND ROBUST WALKING PATTERN FOR PROSTHETIC ANKLE-FOOT UTILISING A NONLINEAR AUTOREGESSIVE NETWORK WITH EXOGENOUS INPUTS

Field of Study: Rehabilitation Robotics

I do solemnly and sincerely declare that:

1. I am the sole author/writer of this Work;
2. This Work is original;
3. Any use of any work in which copyright exists was done by a way of fair dealing and for permitted purposes excerpt or extract from, or reference to or reproduction of any copyright work has been disclosed expressly and sufficiently and the title of the Work and its authorship have been acknowledged in this Work;
4. I do not have any actual knowledge nor do I ought reasonably to know that the making of this work constitutes an infringement of any copyright work;
5. I hereby assign all and every right in this copyright to this Work to the University of Malaya ("UM"), who henceforth shall be owner of the copyright in this Work and that any reproduction or use in any form or by any means whatsoever is prohibited without written consent of UM having been first had and obtained;
6. I am fully aware that if in the course of making this Work I have infringed any copyright whether intentionally or otherwise, I may be subject to legal action or any other action as may be determined by UM.

Candidate's signature   Date
                               27/11/2021

Subscribed and solemnly declare before,

Witness's signature   Date 29/11/2021

Name:

Designation

[GENERATING AN ADAPTIVE AND ROBUST WALKING PATTERN FOR PROSTHETIC ANKLE-FOOT UTILIZING A NONLINEAR AUTOREGRESSIVE NETWORK WITH EXOGENOUS INPUTS]

Abstract

Many challenges are associated with the development of powered lower limb prostheses, ranging from their mechanical design to their control system. Many studies on the use of control algorithms in the field of rehabilitation robotics have attempted to mimic the behavior of an intact lower limb with different walking speeds over diverse terrains and used different control structures and logic to achieve this overarching goal. Recently, most of these studies tend to use a hierarchical control structure with three control levels. This three-level control structure has at least one element of discrete transition properties that requires many sensors to improve classification accuracy. However, these sensors also lead to higher computational load and costs. In this study, a developed artificial neural network capable of generating dynamic control signals of the missing foot, user-independent and free-mode method using minimum sensory feedback signals was proposed to eliminate the need to switch among different controllers. A database was constructed using four OPAL wearable devices (Mobility Lab, APDM Inc., USA) for seven able-bodied subjects. The gait of each subject at three ambulation speeds during ground-level walking was recorded to train a non-linear autoregressive network with an exogenous input recurrent neural network (NARX RNN) for estimating foot orientation (angular position) in the sagittal plane using shank angular velocity as external input. The trained NARX RNN estimated the foot orientation of all subjects at different walking speeds over a flat terrain with an average root mean square error of $2.1° \pm 1.7°$. The minimum correlation between the estimated and measured values was 86% which indicated the high similarity between the estimated and measured foot trajectories. Moreover, results of the t-test show that the error is normally distributed with a high certainty level (0.88 minimum p-value). In addition, the extreme value distribution of the measured

and estimated data of all subjects were quite identical which indicates probabilistic consistency of the model. NARX RNN capability to generate the dynamic control signals for different walking cadences will reduce the risk of amputees falling or stumbling when a wrong classification occurs using the conventional three-level controllers.

Keywords: Powered Ankle-Foot; High-Level Control System; Pattern Generator; NARX Network; ANN; Hierarchical Control System.

[MENJANA CORAK PERJALANAN YANG ADAPTIF DAN TEGUH UNTUK MANFAAT BUKU LALI-KAKI PROSTETIK MENGGUNAKAN RANGKAIAN AUTOREGRESIF BUKAN LINEAR DENGAN INPUT EKSOGEN]

Abstrak

Banyak cabaran dikaitkan dengan pembangunan prostesis anggota bawah berkuasa, dari reka bentuk mekanikalnya hingga ke sistem kawalannya. Banyak kajian tentang penggunaan algoritma kawalan dalam bidang robotik pemulihan telah cuba meniru tingkah laku anggota bawah yang utuh dengan kelajuan berjalan yang berbeza di pelbagai rupa bumi dan menggunakan struktur kawalan dan logik yang berbeza untuk mencapai matlamat menyeluruh ini. Baru-baru ini, kebanyakan kajian ini cenderung menggunakan struktur kawalan hierarki dengan tiga tahap kawalan. Struktur kawalan tiga peringkat ini mempunyai sekurang-kurangnya satu elemen sifat peralihan diskret yang memerlukan banyak penderia untuk meningkatkan ketepatan pengelasan. Walau bagaimanapun, sensor ini juga membawa kepada beban pengiraan dan kos yang lebih tinggi. Dalam kajian ini, rangkaian neuron tiruan yang dibangunkan mampu menjana isyarat kawalan dinamik bagi kaki yang hilang, kaedah bebas pengguna dan mod bebas menggunakan isyarat maklum balas sensor minimum telah dicadangkan untuk menghapuskan keperluan menukar antara pengawal yang berbeza. Pangkalan data telah dibina menggunakan empat peranti boleh dipakai OPAL (Mobility Lab, APDM Inc., USA) untuk tujuh subjek yang mampu. Gaya berjalan setiap subjek pada tiga kelajuan ambulasi semasa berjalan di aras tanah telah direkodkan untuk melatih rangkaian autoregresif bukan linear dengan rangkaian saraf berulang input eksogen (NARX RNN) untuk menganggar orientasi kaki (kedudukan sudut) dalam satah sagittal menggunakan sudut shank halaju sebagai input luaran. NARX RNN yang terlatih menganggarkan orientasi kaki semua subjek pada kelajuan berjalan yang berbeza di atas rupa bumi rata dengan purata punca ralat min kuasa dua sebanyak $2.1°\pm1.7°$. Korelasi minimum antara nilai anggaran dan diukur ialah 86% yang menunjukkan persamaan yang tinggi antara trajektori kaki yang dianggarkan

dan diukur. Selain itu, keputusan ujian-t menunjukkan bahawa ralat adalah taburan normal dengan tahap kepastian yang tinggi (0.88 nilai p minimum). Sebagai tambahan, taburan nilai melampau bagi data yang diukur dan dianggarkan bagi semua subjek adalah agak sama yang menunjukkan konsistensi kebarangkalian model. Keupayaan NARX RNN untuk menjana isyarat kawalan dinamik untuk irama berjalan yang berbeza akan mengurangkan risiko amputasi jatuh atau tersandung apabila klasifikasi yang salah berlaku menggunakan pengawal tiga peringkat konvensional.

Kata kunci: Powered Ankle-Foot; Sistem Kawalan Tahap Tinggi; Penjana Corak; Rangkaian NARX; ANN; Sistem Kawalan Hierarki.

Acknowledgements

TABLE OF CONTENTS

List of Figures

List of Tables

List of Symbols and Abbreviations:

Adam:	Adaptive Moment Estimation
Adagrad:	Adaptive Gradient Algorithm
ADF:	Augmented Dickey–Fuller
AggMo:	Aggregated Momentum
ANN:	Artificial Neural Network
AR:	Ascent Ramps
ARc:	Autoregression coefficients
AS:	Ascent Stairs
BMLP:	Bridged Multilayer Perceptron
BR:	Bayesian Regularization Backpropagations
CD:	Controlled Dorsiflexion
CP:	Controlled Plantarflexion
CPG:	Central Pattern Generator
DBN:	Dynamic Bayesian Network
DFT:	Discrete Fourier Transform
DoF:	Degrees of Freedom
DR:	Descent Ramps
DS:	Descent Stairs
EMG:	Electromyography
EVD:	Extreme Value Distribution
FCC:	Fully Connected Cascade
FSM:	Finite State Machine
FSR:	Force Sensing Resistors
GL:	Ground Level Walking
GMM:	Gaussian Mixture Models
GRF:	Ground Reaction Force
h:	Null Hypothesis
HC:	Heel Contact
HZD:	Hybrid Zero Dynamics
IMU:	Inertial Measurement Unit
LDA:	Linear Discriminant Analysis
LM:	Levenberg–Marquardt
LR:	Logistic Regression
LSTM:	Long Short-Term Memory Neural Network
MAE:	Mean Absolute Error
MB-GD:	Mini-Batch Gradient Descent
MV:	Majority Vote strategy
Nadam:	Nesterov Accelerated Adaptive Moment Estimation
NAG:	Nesterov Accelerated Gradient
NARX:	Nonlinear Autoregressive Network with an Exogenous Input

NBN:	Neuron By Neuron
PCA:	Principal Component Analysis
PEA:	Parallel Elastic Actuator
PO:	Push-off
PP:	Powered Plantarflexion
r:	Cross-correlation
RMSE:	Root-Mean-Square Error
RNN:	Recurrent Neural Network
SEA:	Series-Elastic Actuator
SGD:	Stochastic Gradient Descent
SVM:	Support Vector Machine
SW:	Swing phase
TD:	Time-Domain
TDAR:	Combining Time-domain and Three-order Autoregression coefficients
TO:	Toe-off
ULDA:	Uncorrelated Linear Discriminant Analysis
QDA:	Quadratic Discriminant Analysis
QHAdam:	Quasi-Hyperbolic Adam
y[k]:	is the neural network's normalized output
u[k]:	is the angular speed of the tibia
ω_n:	filter's cut-off frequency
Ts:	is sample time
$r(n,k)$:	maximum number of regions
k:	number of inputs
n:	the number of neurons at the first layer
θ_{foot}:	foot orientation
θ_{tibia}:	shank orientation
W:	weights vector or neural network parameters
η:	the learning rate
C:	the cost function
η_t:	an adaptive learning rate
γ:	momentum term
Δw_t:	weights update vector
$g_{t,i}$:	the gradient at time step t.
$G_{t,ii}$:	is a diagonal matrix, where each diagonal element ii is the sum of the squared gradients.
ϵ:	is a smoothing term
H_t:	is the Hessian matrix
γ_t:	is the conjugate parameter
J_t:	Jacobian matrix

e_t: is the error

μ: is the combination coefficient

I: is the identity matrix

List of Appendices:

CHAPTER 1   INTRODUCTION

1.1 General introduction:

The number of lower extremity amputation procedures has significantly increased over the past 10 to 15 years due to many factors. The majority of the major amputation procedures for lower extremities are performed at the transtibial level, followed by the transfemoral level (McLaughlin, 2018). The number of lower extremity major amputations in the world ranges between 3.6 to 68.4 per 10^5 population (Moxey et al., 2011). In the US alone, approximately 185,000 amputations are being performed each year (Marzen-Groller et al., 2005). These huge numbers only highlight the importance of rehabilitation intervention.

Depression or depressive symptoms have also been reported by some patients as a driver of their poor mobility and reduced use of prostheses shortly after amputation. Patients who underwent long-term amputations also attributed their depression to activity restrictions, overwhelming feelings of vulnerability, and poor self-rated health (Behel et al., 2002; Horgan et al., 2004; Jones et al., 1993).

Over the past few decades, the use of powered prosthetic devices has increased due to their contributions in improving the mobility and quality of life of amputees (Jimenez-Fabian et al., 2012). These prostheses mimic a robust walking pattern comparable to a normal gait cycle. Meanwhile, passive and semi-active prostheses lead to asymmetric gait patterns, have low shock absorption, and increase the metabolic cost (Goldfarb et al., 2013; Waters et al., 1976). Passive prostheses also contribute to joint disorders, chronic residual limb pain, and back pain (Ephraim et al., 2005) and increase the risk of developing osteoarthritis (Burke et al., 1978; Lemaire et al., 1994).

Powered prosthetic devices mostly depend on intermittent non-dynamic control strategies as will be discussed in the literature review. Using these devices exposes amputees to the risk of falling if any wrong classification occurs during ambulation. In addition, these controllers lead to a high computational load, increasing the weight and price of powered prosthetic devices and reduce the comfort of amputees due to the large number of sensors required for reducing classification errors. Furthermore, some of these controllers rely on electromyographic (EMG) signals for intent recognition, some rely on mechanical sensors attached to the prostheses or the bodies of amputees, and others rely on hybrid feedback signals from both types of sensors. Gradual changes in EMG bursts and motor patterns occur with different inclinations of slopes (Prentice et al., 2004). Therefore, more predetermined patterns need to be defined to cover all terrains faced by amputees in their daily use of prostheses, which would require the use of a complex control structure and a highly sophisticated intent recognizer.

(Grasso et al., 2004) found that the recovery of patients with spinal cord injuries mainly depends on the reactivation of a neuro-mechanical circuit response to generate motor patterns. For prosthetic ankles, generating a human-like non-linear oscillatory signal represents an initial step toward restoring the normal walking gait of amputees.

The relationship between tibia kinematics and the desired foot orientation throughout ambulation has been supported by evidence (Holgate et al., 2008; Holgate et al., 2009). Therefore, the foot angular position was estimate based on the angular velocity of the tibia by training a NARX recurrent neural network. NARX is suitable for generating non-linear oscillations associated with locomotion and is more convenient than conventional neural networks in terms of the long term-dependencies in the data (Lin et al., 1996).

1.2 Problem statement:

Passive prostheses are the most commercially available prosthetic devices, due to the hefty price of powered prostheses. The conventional three-level controllers have a non-dynamic intermittent control structure. Where the misclassification exposes the amputees to falling risks. The non-dynamic switching rules of the conventional controllers are limited to certain walking terrains which the intent recognizer is trained to recognize. The conventional controllers require an extensive number of sensors to classify the walking mode and speed which increases the computation load and the cost of the prosthetic device. Most of the conventional controllers are user-dependent, which means special training for the control system is required based on each patient's data before the usage of the powered prosthesis. The alternative methods of the conventional controllers are weather user-dependent, unable to produce different walking cadences, or require a high number of sensors.

1.3 Research objectives:

1. to develop an artificial neuromechanical circuit to generate human-like non-linear oscillatory signals that will replace missing biological signals and restore the normal gait of amputees by using powered ankle-foot prostheses; and

2. to make this artificial neuromechanical circuit user-independent able to generate the desired patterns with minimal tuning before usage by any amputee and make it adaptive to different walking cadences.

1.4 Dissertation outline:

The rest of this dissertation is organized as follows. Chapter 2 reviews the literature.

Chapter 3 describes the methodology. Chapters 4 and 5 presents the results and the related discussion, respectively. Chapter 6 concludes the dissertation and proposes directions for future work.

CHAPTER 2   LITERATURE REVIEW

Emulating an intact lower limb behavior across different speeds and terrains has been an overarching goal of many studies on rehabilitation robots. Therefore, prostheses control systems are mainly categorized based on the motion intention detection techniques of amputees and the inputs utilized in such techniques (J. Martin et al., 2010).

The motion intention of amputees can be recognized using various sensory feedback signals (e.g., neuromuscular activates, locomotive state, or physical interactions with the environment or the prosthesis) that may be fully embedded onto highly invasive sensors (e.g., surgically implanting electrode arrays). Accurately classifying motion intention is critical in preventing injuries related to falls and unstable walking. Therefore, maximizing the richness of information and minimizing the number of invasive sensors are crucial (Tucker et al., 2015), and further research must be performed to accurately and intuitively recognize the motion intention of amputees. In this chapter a thorough review of the control systems used in the literature is made. First, it starts with the two-level controllers, more specifically the echo controller as it is the first published control system developed for powered prostheses in 1977. Then, the FSM two-level controllers, these controllers are initial for the understanding of the conventional three-level controllers. Second, the review covers the three-level conventional controllers comprehensively. Where, the classification algorithms and the sensors used for intent recognition were described, starting with biomechanical-based intent recognizers, to the EMG-based intent recognizers and capacitive modulation-based intent recognizers, ending with neuromuscular-mechanical fusion-based intent recognizers. Third, many alternative methods were presented. First, the inverse dynamic control strategies. Second, biological-signals-inspired controllers. Two methods were introduced in

the literature. One is the central pattern generator-based controller. Second, the LSTM RNN based control strategies.

2.1 Two levels control strategies

The echo control strategy is among the first approaches used in powered transfemoral prostheses (Flowers et al., 1977; Grimes et al., 1977). In this method, prosthesis simply duplicates the motion patterns of the sound leg. Mechanical sensors are mounted on prostheses to provide feedback signals as variables for timing function switches between controlling modes. However, this strategy does not observe various walking terrains and is not accurate enough in phase detection.

A more efficient approach that applies a two-level control system was developed for both transtibial and transfemoral prostheses to regulate ambulation over ground-level terrains. This approach achieves a faster information flow and less switching delays compared with the echo control strategy. In this approach, the prerecorded kinematics or kinetics (or both) of an able-bodied human during normal ambulation are used as reference inputs to adjust foot orientation. Signals are executed by a finite state machine at the high level depending on the phase-state of the prostheses, and then the corresponding low-level controller is used to imitate the behavior of biomechanical limbs throughout the gait cycle. (Sup et al., 2007) introduced a prosthetic transfemoral device driven by two pneumatic actuators. FSM regulates the parameters of impedance control throughout ambulation based on different phase walking modes (Stance 1, Stance 2, Swing 1, and Swing 2). In addition to a three-axis socket load cell, position and torque sensors are used in phase detection and for tracking foot trajectory. (Gao et al., 2019) proposed a similar control strategy for controlling a non-linear parallel elastic actuator (PEA) that drives transtibial prostheses. Such prosthetic

device can work in both passive and active modes. In the active mode, the driving circuit controls the motor to drive the prosthetic device and provide a positive mechanical power to the user. When the battery is drained, the circuit works in the passive mode, makes the motor function as a generator, and produces a damping force to avoid foot drop. In the passive mode, a driving circuit is used. Unlike other studies where the state is instantly changed after reaching a fixed condition, (Gao et al., 2019) proposed a threshold technique where the state changes depending on the motion of the user.

(S. K. Au et al., 2007) examined the design and control requirements of transtibial powered prostheses. In accordance with the design requirements derived from intact ankle behavior throughout level-ground walking, they integrated five mechanical elements into their prosthetic prototype, namely, a brushed DC motor, transmission mechanism, series spring, unidirectional parallel spring, and carbon composite leaf spring prosthetic foot. The components are combined to form a controllable series-elastic actuator (SEA), which modulates stiffness through the stance phase and provides a constant torque during plantar flexion. To control SEA through ground-level ambulation, the authors used an FSM control strategy, which has six states representing the ankle joint behavior during ground-level walking. These states include controlled plantar flexion (CP), controlled dorsiflexion (CD), and powered plantar flexion (PP) during the stance phase and SW1, SW2, and SW3 during the swing phase. Three low-level controllers were activated based on the walking state to control the actuator. First, the torque controller was used in PP to generate an offset force. Second, an impedance controller was used in CP and CD to modulate joint stiffness. Third, a position controller was used in the swing phase to control ankle orientation. Three sensors were used to switch between states, namely, foot switches to measure heel/toe contact, an ankle joint encoder to measure ankle angle, and a linear spring potentiometer to measure joint

torque. The authors found that the powered ankle prosthesis can mimic the torque-ankle behavior of an intact human ankle joint. By measuring the oxygen consumption of three amputees, they found that the powered ankle prosthesis reduced their metabolic rate by 7% up to 20% compared with conventional passive prostheses.

(Sun et al., 2014) designed a transtibial prosthesis based on the four-bar mechanism driven by a brushed DC motor and torsional spring. They applied the high-level FSM approach to determine if the prosthesis was in either the stance or swing phase based on its contact with the ground or the ground reaction force measured by a force sensing resistor. If the prosthesis in the stance phase, then the low-level controller is working under the moment control mode. Otherwise, the controller is working under the position control mode during the swing phase. They divided the stance phase into three subphases, namely, loading response, mid- and terminal stance, and pre-swing. The predetermined moment/position profile of an able-bodied person was used as the reference input of the PI/PID low-level controllers. Sensors were used to provide the required sensory feedback to the low-level controllers, an incremental encoder was used to provide the position and angular velocity data to the PID position controller during the swing phase, and a current sensor was used to provide feedback signals to the PI moment controller during the stance phase.

(Cherelle et al., 2014) designed another four-bar-based transtibial prosthesis comprising a brushed DC motor, a ballscrew connected to a lever arm with two tension springs (push-off springs (PO)), and a plantar flexion spring (PF) located between the lever arm and foot. In addition to the current sensor, the load cell force, linear potentiometer, force sensing resistors (FSR), and two magnetic encoders were used to provide the control system sufficient feedback signals. The mechanical design of the prosthesis and the locking mechanism of the lever arm both greatly influenced the control strategy and energy

8

consumption of the system. The control strategy also involved the application of FSM at the high level, and the PI moment controller worked along with the PID position controller at the low level.

(Wang et al., 2014) designed a transtibial prosthesis driven by a brushed DC motor. A load cell, angle sensor, and two inertial measurement units (IMU) were mounted on the prosthesis to provide the required feedback signals for both the high-level FSM controller and low-level controllers (including the damping, torque, and angle controllers). They combined CP and CD into controlled flexion (CF) and then divided the controlled gait cycle into three phases, namely, CF, PP, and SW. The low-level controller worked under the damping control mode in CF, under the torque control mode in PP, and as a position controller in SW.

(Ficanha et al., 2015) built a prosthesis with two degrees of freedom (DoF) that was driven by two brushed DC motors and can function in both frontal and sagittal planes. They used strain gauges to estimate the ground reaction torques and designed two encoders for each motor to measure foot orientation in two dimensions. They applied the FSM approach to monitor the development of admittance and impedance controllers for the ankle-foot prosthesis based on position and torque feedback. However, this prosthesis was difficult to control because the control system must track the movement and determine the phase-state in two planes to switch between low-level controllers in both dimensions. Moreover, developing intent recognition and working over different terrains require the use of highly sophisticated controlling algorithms and an advanced micro controller for data processing.

To the best of my knowledge, all controlling techniques based on the two-level control strategy are only capable of controlling prostheses over a single walking terrain. However,

the FSM-based two-level controlling strategy is critical given its role as the core of the hierarchy three-level control strategy, which is the most commonly applied approach in the literature.

2.2 Three-levels control strategies

In three-level control strategies, an intent recognizer acts as a high-level supervisory controller that switches among different tasks, including ground-level walking (GL), ascend/descend ramps (AR/DR), or ascend/descend stairs (AS/DS), etc. Each task is performed using FSM in the mid-level control, in which the prosthesis state is observed and the desired command is transmitted to the proper low-level controller(s) (Tucker et al., 2015). The three-level control strategies adopted in the powered prostheses literature differ in their use of high-level control as an intent recognition technique and their chosen sensory feedback for intent recognition (i.e., EMG, mechanical sensors, or capacitors). This section categorizes the controllers based on their utilized intent recognition techniques (i.e., the classification algorithm and the feedback signals used for intent recognition). Figure 2.1 illustrates the general three-level control structure used in these studies.
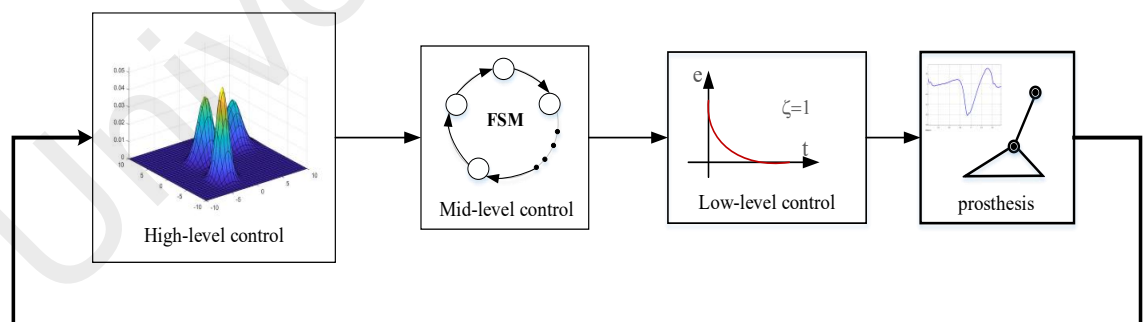
Figure 2.1: Block diagram depicts the hierarchical three-levels control strategy used to control most of powered prosthetic devices.

2.2.1 Intent recognition based on biomechanical feedback:

In this method, mechanical sensors are attached to prostheses to recognize the intention and identify the walking modes of amputees. Controlling algorithms relying on biomechanical

10

feedback have low costs and computational loads given the small number of sensory feedback signals that need to be processed and their properties (i.e., high amplitude, noise resistance, and continuous feedback signals). Moreover, the sensors used to collect these signals are non-invasive, do not affect the comfort of amputees, and do not require the wearing of additional instruments apart from prostheses. However, this method has a higher classification error and longer transition delay between two tasks compared with other methods.

Over the past two decades, the Vanderbilt University published many studies on the development of ambulation mode intent recognition based on mechanical sensory feedback for both transfemoral and transtibial prostheses. For instance, (Sup et al., 2009) designed a transfemoral prosthetic device driven by two brushless DC motors and relies on five strain gages, two potentiometers, ankle and knee current sensors, and a three-axis accelerometer to observe the states and their interaction with the environment and the residual limb and to provide the three-levels control system with sufficient feedback signals. They tested their prosthesis on ground-level walking with three different speeds and standing still and used the same Gaussian mixture models (GMM) supervisory controller as in their former pneumatic prototype (Varol et al., 2008). A total of 100 samples-long frames were generated from 7 sensor signals, the mean values and standard deviation were computed, and a 3D principal component analysis (PCA) algorithm was used to reduce the dimension of the collected data to be analyzed by the 7-mixture GMM classifier. A voting vector length of 38 was then used to minimize delay in gait mode intent recognition (Figure 2.2). A transition period of 0.4 to 0.5 seconds was observed between two modes, which is convenient for real-time implementation. Unlike in previous studies, (Varol et al., 2009) used 3D linear discriminant analysis (LDA) for dimension reduction. LDA outperformed PCA in the standing, sitting,

and walking cases. They also used GMM with 6 mixtures and a voting vector length of 45 to recognize user intent. Some classification errors were observed during the experiment, which the authors argued was not problematic and not perceivable by the user. The execution time of their identification method was slightly longer than those of other methods given that more classes need to be identified.
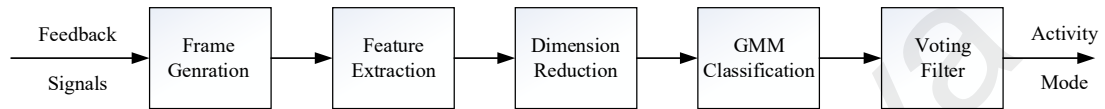
Figure 2.2: A flowchart emphasizes the procedure of intent recognition

(Sup et al., 2010) developed a control system that allows their designed transfemoral prosthesis to walk up slopes and then compered their results with the native trajectories of able-bodied subjects and passive prosthesis trajectories. In contrast to previous studies that distinguish walking from standing, (Sup et al., 2010) did not use any classification, dimension reduction, or voting vector methods to identify the intent of their subjects to walk up slopes. Instead, they used a basic threshold algorithm based on gravity orientation that utilizes a three-axis accelerometer. The controller only determined $5°$ and $10°$ slopes, and the authors claimed that the $\pm 2.5°$ variation of slopes does not require the alteration of prosthesis behavior and that the building codes in the US limit the maximum incline of a ramp to approximately $5°$. Using second-generation transfemoral prosthesis, the authors implemented their developed controller for stairs ascent and descent as described in (Lawson et al., 2012). However, they only described their FSM strategy for stairs ascent and descent and compared their results with those for passive prosthesis and healthy subjects without mentioning the identification techniques they used to switch between activity modes.

(Shultz et al., 2015) proposed an algorithm for controlling their designed transtibial powered prosthesis, which is similar to their former method for controlling transfemoral

prosthesis. However, their high-level controller was simple and able to identify the activity modes through a predetermined offset angular position, the velocity of the ankle as provided by the encoder, and the angular position and velocity of the shank as observed by the IMU unlike previous studies that rely on ground reaction force (GRF) observations and the positions of ankle and knee joints, which are fed to a GMM-based classifier to recognize user intent and initiate the proper pattern. To switch between different walking speeds, the time between each heel strike was recorded, and the high-level controller would switch to the control parameters that correspond to the walking speed of the subject with a 2 step/min hysteresis in order to mitigate chatter between sets of control parameters. Meanwhile, to switch between activity modes (i.e., walking or standing), the high-level would switch from standing to walking mode when the ankle prosthesis reaches a predetermined angle offset through dorsiflexion. Therefore, a transition from standing to walking mode can only occur between the support state of standing and the late stance phase of walking. Meanwhile, switching from walking to standing mode is only possible between the middle stance phase (walking) and the support phase (standing) when the absolute angular velocity of the shank is near 0 for 0.5s.

(Young et al., 2015; A. J. Young et al., 2014; Young et al., 2013) estimated ambulation mode intent by using 13 mechanical sensors embedded on a powered transfemoral prosthesis that includes potentiometers and encoders at the knee and ankle, an axial load cell, and a six-axis IMU on the shank (same prototype introduced in (Lawson et al., 2012) built by Vanderbilt University). Data of six unilateral transfemoral amputees were collected during 20 repetitions of a circuit. These data included walking on level ground and on a ramp with a $10°$ slope and ascending and descending a four-step staircase using reciprocal gait (Young et al., 2013). These data were divided into eight points during the gait

cycle, and the data before each toe off and heel contact events were segmented into variable window sizes to test the performance of the intent recognition system for each window size. Four features, namely, mean, standard deviation, maximum, and minimum, were calculated within each window for all signals from those feedback signals that form a feature vector size 52. Afterward, an LDA algorithm was used for dimension reduction (Varol et al., 2009). The authors also evaluated the effect of training the intent recognizer with one to multiple analysis windows (majority vote strategy (MV)) and assessed the classification performance during both transition and steady states by calculating the percentage of misclassifications recorded during the transitions and the steady state. In their statistical analysis, the authors found that a single analysis window at heel contact and toe off with 250 ms length generates the most accurate outcomes. Moreover, training the intent recognizer using the data obtained during the transitions can lead to significantly more accurate results than training the intent recognizer using steady state data. (A. J. Young et al., 2014) extended their previous work by introducing a time history with dynamic Bayesian network (DBN) strategy for walking mode recognition. The technique using DBN obtained a lower classification error compared with MV- and maximum-likelihood-based techniques, whereas the MV-based technique demonstrated the worst performance. Data from eight unilateral transfemoral amputees were then used to develop a user-independent intent recognizer (Young et al., 2015), where the data of seven subjects were used to train the pattern recognition system, and the data for the eighth subject were used to test classification performance. Results were then validated across all subjects. The data were segmented into 8 windows with 300 ms width, and the extracted features from each window were expanded into 6 features by adding the starting and ending signal values to the 4 features used in their previous study. They also introduced two other classification strategies, the first of which is mode-specific configuration, in which a separate LDA classifier is used for each locomotion mode without any time history

14

information. Figure 2.3 shows the block diagram of this strategy. The other strategy is the mode-specific + time history configuration, which combines the mode-specific and DBN time history strategies. The same eight windows are used in the analysis for prior probability propagation. However, separate DBN classifiers are used based on the previous locomotion mode. Both the mode-specific and mode-specific + time-history classifier configurations obtained significantly less transitional errors than the baseline and time-history classifiers. However, in terms of steady-state classification error, the time history DBN-based classier and the mode-specific + time history classifier significantly outperformed the mode-specific and baseline classifiers. Meanwhile, the user-dependent classifiers outperformed user-independent classifiers in terms of transition steps and user-independent steps. However, the classification error of the user-independent classifier decreased when the combined data for training increased from one to seven subjects. The authors argued that including more subjects to the combined training data may enhance the classifier performance. Developing a user-independent classifier or controller for prosthetic devices is considered a critical approach that can reduce training time and satisfy the demands of both patients and clinicians.
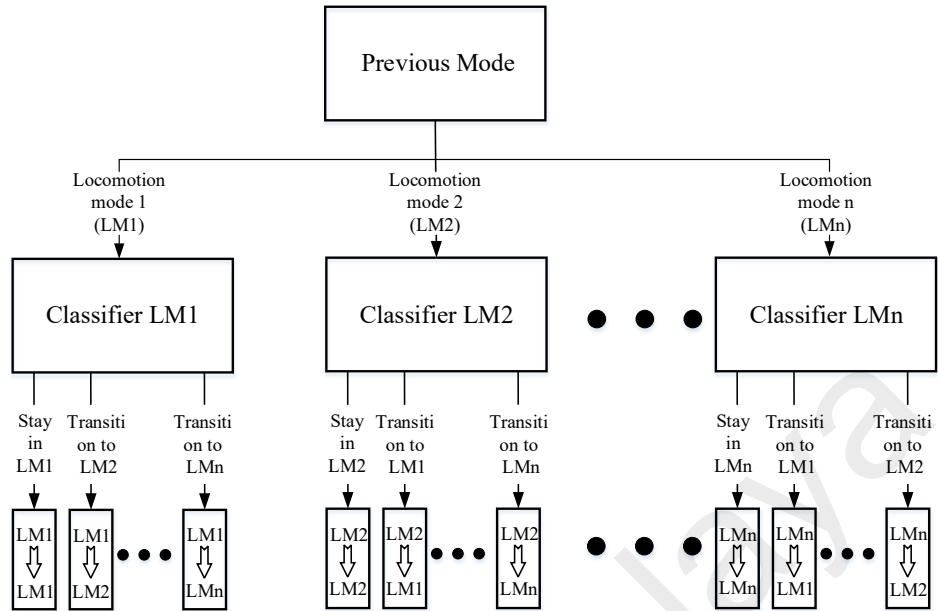
Figure 2.3: Block diagram illustrates Mode-Specific Configuration strategy for locomotion mode classification.

(Yuan et al., 2014) proposed a real-time fuzzy-logic-based intent recognizer to identify the walking mode for a transtibial prosthesis. They used two three-axis gyroscopes, two three-axis accelerometers, two force-sensitive resistors, and a timer to measure the prosthesis state and its interaction with the environment to obtain the required features (i.e., foot inclination angle at first strike, shank inclination angle at first strike, foot strike sequence, foot inclination angle at mid-stance, and shank inclination angle at toe-off) that would allow the fuzzy-logic system identify the walking mode. Three membership functions were used, namely, two hyperbolic tangent functions and one Gaussian function. Two of these functions were used for every feature with different parameters. This fuzzy-logic-based intent recognition algorithm was able to identify five different terrains, namely, LG, RA, RD, SA, and SD, after testing on six able-bodied subjects and three transtibial amputees. The algorithm obtained an average identification accuracy of 98.74%±0.32% (mean±standard deviation) during steady state locomotion, and the average transition delay between 2 walking modes for the 8 transition cases was 9.06%±3.46% for one gait cycle with a

0.79±0.02 ms execution time. (Yuan et al., 2014) also studied the influence of stair height and ramp inclination angle on identification accuracy and found that the recognition performance decreases along with stair height, whereas the variation in ramp inclination angle has a negligible effect on identification accuracy. The transition delay between two walking tasks was almost the same for all transitions, except for that between level ground walking and ramp descent with a low inclination angle, which was significantly longer due to misidentification. Although its accuracy decreases along with varying stair height and ramp inclination angle without taking variations in speed into consideration, this identification algorithm remains applicable in real-time prosthesis control given its ability to identify most of the common terrains faced by the amputees with higher accuracy and shorter transition delays compared with other methods.

(Stolyarov et al., 2017) developed a method that predicts locomotion mode by using the translational motion derived from IMU data. They collected their data using a six-axis IMU and a 12-camera Vicon 8i motion capture system from 6 transtibial amputees while preforming five walking tasks (LG, RA, RD, SA, and SD). Three separate features sets were extracted from the collected IMU data, including the raw sensed data, knee and ankle translational motion signals derived from the sensed data, and expanded features comprising both sensed data and translational motion. Each feature set includes the maxima, minima, means, and standard deviations extracted from associated signals in the analysis window. The authors then compared the performance of the LDA-based intent recognizer using three sets of features and found that the translational motion features set significantly outperformed the sensed and expanded features sets with a high prediction accuracy (composite error of 4.7%). Using translational data for intent recognition is also computationally feasible for real-

time implementation. The proposed method can also predict walking tasks independent of walking speed, prosthesis, and subject.

2.2.2   Intent recognition based on electromyography feedback:

Previous studies have commonly used EMG signals measured from the residual limb as feedback signals for the controllers of powered lower limb prostheses. For instance, (S. K. Au et al., 2005) estimated ankle movement intent from EMG signals by using two techniques, the first of which is the biomimetic technique based on the simulated dynamic of the missing limb and the second of which is a technique that uses a standard multilayer neural network. In their analysis and comparison, they found that both controlling techniques can qualitatively estimate the desired ankle movement patterns. However, the biomimetic EMG controller demonstrates a smoother and more natural movement pattern compared with the neural-network-based technique. Meanwhile, (S. Au et al., 2008) used a feed-forward neural network with a single hidden layer to manage the switching between two FSMs in the mid-level, which represent level-ground and stair descent walking patterns. They divided the swing phase into three and two subphases for level-ground walk and stairs descent, respectively. In the second swing subphase (SW2), in both walking modes, the amputee was allowed to voluntarily control the equilibrium position of his/her foot based on residual limb muscular activities. The EMG signals collected by three pairs of surface electrodes were filtered and amplified to generate the input signals of the neural network, which has a binary output (if $y = -1$, then $\theta_{EMG} = -0.35$ rad, else $y = 1$ $\theta_{EMG} = 0$ rad). After estimating the motion intention by using the neural network based on the flexion of appropriate muscles, the new motor state persists until another muscle flexion occurs, which represents the intent of the user to switch to the other walking mode.

(Huang et al., 2008) used a phase-dependent EMG intent recognizer (where a specific classifier is used for each phase; Figure 2.4) to identify 7 locomotion modes, namely, level-ground walking, stepping over an obstacle, ascending stairs, descending stairs, ipsilateral turning, contralateral turning, and standing still. A total of 4 analysis windows with 140 ms length and 30 ms window increments were derived from the gait cycle and aligned with two gait events (i.e., heel strike and toe off). An independent classifier was used for each phase window, and a phase detection module detects the gait events and switches on the associated classifier. They also analyzed different classifier types, EMG features, subsets of EMG channels, length and increment size of the analysis window, and their influence on classification error and response time.
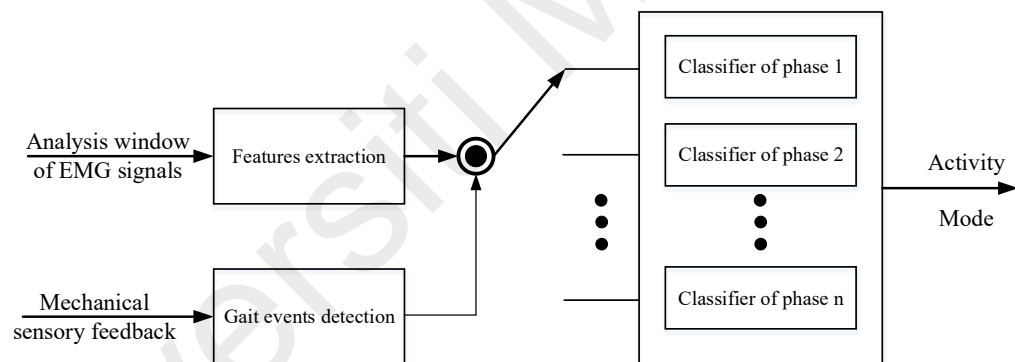
Figure 2.4: Block diagram depict the structure of phase-dependent EMG pattern classifier.

They found that the LDA classification strategy slightly outperforms and is more computationally efficient than the ANN classification strategy for all analysis windows. However, both classifiers fail to accurately classify the walking mode when using the EMG signals of the entire stride cycle. (Huang et al., 2008) also found that analysis window length significantly affects the classification error yet has a negligible influence on the compared EMG features (time domain TD, three-order autoregression coefficients ARc, and their combination TDAR). When using only the EMG signals from muscles in the residual limb (gluteal and thigh muscles), the overall errors in the four phases (Post-HC, Pre-TO, Post-TO,

and Pre-HC) were 19.0%, 19.0%, 8.6%, and 6.7% for the first patient and 22.9%,17.1%, 8.5%, and 12.9% for the second patient, respectively. The lowest classification accuracy was reported in the Post-HC phase for level-ground walking, stepping over an obstacle, and turning. Meanwhile, stair ascent and descent were the most robustly recognized locomotion modes in all phases. However, the transition accuracies of the intent recognizer were not examined.

Although EMG signals appear prior to motion (Yuan et al., 2014) and contain rich information about the state of the amputee (Hargrove et al., 2009), EMG-based motion recognition has some major drawbacks. For instance, low-amplitude signals can be easily affected by external noise, are difficult to measure (Chen et al., 2013), and have non-linear and non-stationary characteristics (S. K. Au et al., 2005; Farry et al., 1996). In addition, sweaty skin and misplacement due to don and doff can negatively impact the signals (Spanias et al., 2018).

2.2.3   Intent recognition based on capacitive modulation

(Chen et al., 2013) developed a new intent recognition strategy that uses capacitive sensory feedback as an alternative model for EMG-based intent recognition. This strategy was later improved by (Zheng et al., 2014) by adding non-contact capacitors. These strategies have addressed many problems associated with classification techniques that use EMG signals, such as their low amplitude and physiological effects. However, the different shapes of amputees' residual limbs may affect the placement of capacitors and require a special training of the classifier for each individual, which is inconvenient for prosthetic technicians. Moreover, the authors ignored the real-time transitions between the walking modes of the classifier. Specifically, (Chen et al., 2013) used 10 channels of the sensing band mounted on

the thigh of the amputated leg to identify 6 locomotion modes (i.e., ground-level walking, ascending/descending stairs, ascending/descending slopes, and avoiding obstacles). They used a phase-dependent classification algorithm with the MV technique, where the phase size, window size, and window increment were set to 190, 150, and 20 ms, respectively. Afterward, they compared the performance of three classification techniques (LDA, logistic regression (LR), and quadratic discriminant analysis (QDA)) and found that LDA slightly outperformed LR, whereas QDA demonstrated the worst performance. The feature set derived from the analysis window for the LDA classifier included mean, maximum, minimum, and root mean square error (RMSE) values. The overall classification accuracies for the five amputee subjects were 94.4±1.5%, 94.0±1.4%, 92.1±0.8%, and 93.3±0.8% for pre-foot contact, post-foot contact, pre-foot off, and post-foot off, respectively. Meanwhile, (Zheng et al., 2014) tested and evaluated their non-contact capacitive sensing system for locomotion intent recognition on six transtibial amputees and used six sensing channels to create the classification features set for identifying six locomotion modes (i.e., ground-level walking, ascending/descending stairs, ascending/descending slopes, and standing). These features were derived from an analysis window with 250 ms length and 10 ms increment along two walking phases (swing and stance). They also compared three classification techniques (LDA, QDA, and two-mixture GMM) to identify the most suitable technique. They found that QDA and two-mixture GMM almost demonstrated the same performance, whereas LDA obtained the lowest classification accuracy. They eventually used QDA because of its lower computational load relative to two-mixture GMM. The average recognition accuracies obtained from six time-domain features were 96.3% and 94.8% for the swing and stance phases, respectively. Although the proposed technique addresses many sensing band problems, such as the negative effects of sweating and dressing/undressing of the band, the non-contact version deals with significantly lower capacitance amplitudes (with

21

average peak-to-peak capacitance ranging from 10 pF to 20 pF). This technique is also affected by residual limb shape and requires the application of three filters in series to regulate the capacitance signals.

2.2.4 Intent recognition based on neuromuscular-mechanical fusion sensory feedback

(F. Zhang, DiSanto, et al., 2011) developed the first intent recognizer, which relies on neuromuscular-mechanical fusion sensory feedback. This recognizer identifies three locomotion modes, namely, level-ground walking and ascending/descending stairs. A total of 11 surface EMG electrodes were fixed on the residual thigh of the user to measure EMG signals, whereas 6 DOF load cells were mounted on the prosthetic pylon to measure mechanical forces/moments. The measured data were segmented by sliding analysis windows with 150 ms length and 20 ms increment. Sets of features were derived from each analysis window. The authors then evaluated the performance of two classification techniques, one of which uses the EMG time-domain features (e.g., mean absolute value, number of zero crossings, number of slope sign changes, and waveform length) and time-domain features extracted from the measured mechanical sensors (the mean, minimum, and maximum values). Meanwhile, the other technique uses EMG time-frequency-domain features (extracted by wavelet packet decomposition, with the number of features depending on its depth) and the time-domain features of the mechanical sensors. Although the first technique outperforms the other, the authors stated that the latter may outperform the former when more walking tasks are considered. The derived features were reduced by PCA before being fed into a phase dependent LDA classifier. Results show that the neuromuscular-mechanical fusion technique has better classification accuracy (99.73% during steady-state) than the other classification techniques that only rely on mechanical or neuromuscular feedback. (F. Zhang, Dou, et al., 2011) expanded their study to include two additional tasks

for the intent recognizer to identify (i.e., standing and sitting). They reduced the number of EMG channels to 10 and increased the window increment length to 50 ms. They also replaced the LDA classifier with a support vector machine (SVM), a non-linear kernel classification algorithm, but used the same features set. They tested their recognition system on a transfemoral amputee and reported an average steady state classification accuracy of 98.36% for all tasks. The intent recognizer also detected all transitions between the tasks before the critical timing for switching the control of prosthesis.

(Huang et al., 2011) trained and tested their recognition system on five transfemoral amputees across six locomotion modes (i.e., ground-level walking, ascending/descending stairs, ascending/descending slopes, and stepping over an obstacle). They used the same phase-dependent SVM classifiers and classification features sets in their previous studies. However, they increased the number of EMG channels to 16 and reduced the window increment length to 12 ms. The steady-state classification accuracies in the stance and swing phases exceeded 99% and 95%, respectively. All types of transitions were accurately identified within the defined prediction time of stable mode transitions.

(A. Young et al., 2014) used the dynamic Bayesian network DBN strategy for intent recognition for five locomotion modes (i.e., level-ground walking, ascending/descending stairs, and ascending/descending slopes). They collected their training and testing data from six subjects with unilateral transfemoral amputations and two subjects with knee disarticulation amputations. Data from 13 mechanical sensors (with the IMU, load cells, and kinematic sensors determining the positions and velocities of the knee and ankle) and 9 surface EMG electrodes were segmented by analysis windows with 300 ms length prior to 8 walking events along the walking gait. They also derived the same time-domain classification feature sets from each analysis window as in previous studies. The results obtained by this

classification technique outperformed those obtained by other techniques. The authors also statistically demonstrated how the data derived from mechanical and neuromuscular sensory feedback can lead to a more accurate mode classification. The average classification accuracies of the developed intent recognizer were 99% and 87.7% during steady state and transitions, respectively.

(Liu et al., 2015) developed and tested an environment-aware locomotion mode recognizer. They used IMU data and laser distance meter sensors mounted on the waist of the subject to recognize the upcoming terrain. Such information was employed in the neuromuscular-mechanical fusion recognition system presented in (Huang et al., 2011; F. Zhang, Dou, et al., 2011) to accurately identify the walking mode. The authors also used a decision tree algorithm to detect the terrain change in front of the wearer. This strategy determines the terrain change before the execution of locomotion mode transitions with more than half second. The environmental information was modeled as a supplementary source for the locomotion mode recognizer in order not to dominate the decision making in locomotion mode classifiers. In this way, no classification errors will be observed when the terrain recognizer misidentifies the next walking mode unless both the locomotion mode and terrain recognizers encounter the same error. Results of this strategy highlighted significant improvements in classification accuracy for both coarse (3.4% to 6.2%) and refined (4.8% to 8.0%) terrain recognition. The authors did not report any missed transition when using the locomotion mode recognition system integrated with the coarse or refined output of the terrain recognition module throughout the 196 transitions during their experiment. This intent recognition strategy outperformed all former neuromuscular-mechanical fusion strategies with a negligible increase in computation burden.

Similar to (A. Young et al., 2014), (Spanias et al., 2018) used the DBN technique for intent recognition and developed an adaptive forward prediction algorithm to overcome the problem where EMG signals change during daily prosthesis use. Eight unilateral transfemoral amputees were asked to perform six locomotion modes (i.e., standing, level-ground walking, ascending/descending stairs, and ascending/descending slopes), and their collected data were used for training and testing the developed intent recognition system. Eight EMG electrodes were used to collect the reaction of residual limb muscles during ambulation for each subject, and 22 mechanical sensors were embedded to measure the kinetic, kinematic, and inertial signals. The same time-domain feature sets were derived from the measured data as in the previously mentioned studies. However, the authors used the uncorrelated linear discriminant analysis (ULDA) technique to reduce the dimension of the feature set from 132 to 13. The mechanical and EMG feature sets were treated independently to identify the adaptation procedure for the EMG data. Unlike in previous studies, the intent recognizer was tested over multiple days to determine whether the adaptive algorithm can identify when EMG should be incorporated into its forward predictions. Results showed that the adaptive algorithm can learn how to reincorporate EMG signals into the intent predictions of the recognizer, but interestingly, the benefits of including EMG were negligible given the improvements already made to the control system (a 0.01% increase for steady state error, and a 0.10% increase for transitional error). Accordingly, the authors suggested that EMG signals may not be necessary for intent recognition in powered lower limb prostheses, and other approaches, such as improving the classifier architecture, the selection of mechanical sensors, or the timing of mode transitions, can provide similar benefits to EMG signals.

In sum, although neuromuscular-mechanical fusion intent recognizers may improve classification performance, they require the installation of many electrodes on the residual

limb and some mechanical sensors, such as load cells, IMU, or laser distance meters, which may affect their acceptance by users and increase computational load. Moreover, similar to other intermittent control systems, amputees are placed at risk of falling when the upcoming terrain is not accurately predicted.

2.3 Inverse dynamic control strategies

The aforementioned control systems share the same problem of intermittent, non-dynamic switching rules between tasks and phases, which place the amputees at risk of falling in case of any wrong recognition arises due to perturbation Moreover, tuning the parameters of these control systems spends many hours providing the controllers with the appropriate parameters for each individual (Simon et al., 2014). Many studies have attempted to develop alternative control systems to overcome these drawbacks, one of which is the hybrid zero dynamics (HZD) controller (Gregg et al., 2014; A. E. Martin et al., 2017; Quintero et al., 2017) , which is commonly used in bipedal and humanoid robots and has been demonstrated to generate stable walking patterns (Chevallereau et al., 2010; Chevallereau et al., 2005; A. E. Martin et al., 2014; Ramezani et al., 2014; Tlalolini et al., 2010; Westervelt et al., 2018). However, HZD-based controllers with the formulation presented in bipedal robots are not applicable to prosthetic systems where the sensors embedded to the prosthetic device only provide information about the state of the device. In addition, the two dynamic systems (the bipedal, and human-prosthesis systems) are incompatible ,where the human-prosthesis system is a coupled non-linear dynamic system, whereas bipedal robots, unlike prosthetic systems, accumulate feedback about the full bipedal state and follow a constant periodic trajectory in contrast to the normal human body gait. To implement HZD in powered prostheses, an input-output linearizing controller must be developed for the coupled periodic mechanical (human-prosthesis) system. Moreover, the control system must be robust to human-like kinematic

variations. This strategy relies on the inverse dynamics of the human-prosthesis system, and the interaction force between the human body and the prosthesis, which represents the effects of one subsystem on another, can be used in the prosthesis controller to account for human dynamics. (Gregg et al., 2014; A. E. Martin et al., 2015, 2017; Quintero et al., 2017) developed a mathematical dynamic model of above-knee amputees including their prosthetic device, which is represented by seven leg segments and a point mass at the hip. They derived the interaction force between subsystems from the dynamic model for the simulation. Nonetheless, the interaction force can be measured directly from the socket during the practical implementation of the controller. An algebraic mapping was used to model the two impact periods during the transition of the contralateral or prosthetic leg to the stance phase. To apply the input-output linearizing controller, the output functions should characterize the desired kinematics of the actuated joints. To this end, four output functions were used to represent each leg for different stance periods. For each function, the authors supplemented a phase variable to represent the progression through the step and captured the motion of the unactuated DoF. They used Bézier polynomials in their first studies to parametrize the output functions (i.e., the virtual constrict or desired trajectory), whereas in their latest study (Quintero et al., 2017), they converted these polynomials by the 10th-order unified discrete Fourier transform (DFT), thereby eliminating the four output functions and the algebraic mapping during the impact. The periodic DFT generates the knee and ankle trajectory in a continuous form along the gait cycle unlike the Bézier polynomials, which immediately diverge to unbounded values and require an accurate phase detection. Moreover, the unified DFT controller had more rustiness than the piecewise HZD controller to speed perturbations. Despite providing a dynamic and continuous control of the prothesis and taking the human gait variability within one walking mode into account, this approach ignored the variations in the inertia of the human limbs and the difference between the dynamics of walking tasks

(e.g., running involves a flying phase in contrast to other tasks (Chevallereau et al., 2005). Therefore, further developing this controller in the future may pose a huge burden when such device is supposed to work for different walking tasks and individuals.

2.4 Biological-signals-inspired controllers

Biological-signals-inspired controllers emulate non-linear central biological signals. Similar to inverse-dynamic-based controllers, these controllers aim to overcome the problems associated with the prevalent hierarchical controllers. For above-knee prostheses, (Nandi et al., 2008) implemented an artificial recurrent neural network called central pattern generator (CPG), which has been widely used in bipedal robots (Di Canio et al., 2016; Inada et al., 2003; Morantes et al., 2016; Taga et al., 1991; Yakovenko et al., 2018). However, a suitable CPG neural network needs to be designed based on the height, weight, and age of each amputee. CPG also has a sophisticated parameter calibration process, which poses additional challenges given that the human gait is not completely periodic, has a highly coupled dynamic and chaotic nature, and has no fixed patterns. The human gait also varies between walking tasks, thereby requiring the development of a specific CPG neural network for each task or training this network to be adaptive to different candace and walking patterns. Therefore, a more complex and sophisticated learning algorithm is required.

(Rai & Rombokas, 2019; Rai, Sharma, et al., 2019) designed a recurrent long short-term memory neural network (LSTM RNN) to estimate the ankle angle of the amputated leg based on the kinematics of the intact and residual limbs. However, in this strategy, the number of sensors (6 to 17 sensors attached to the body of the subject in addition to the sensors embedded in the prosthesis) and neurons (244) in the RNN increases the cost of the device, leads to greater time and power consumption, and reduces the comfort of subjects.

CHAPTER 3 METHODOLOGY

The control system (pattern generator) can be divided into experimental settings, data analysis, and artificial neural network (ANN) design. Meanwhile, the ANN development involves topology selection, training, and performance assessment. Figure 3.1 is the flowchart of the method in this study.
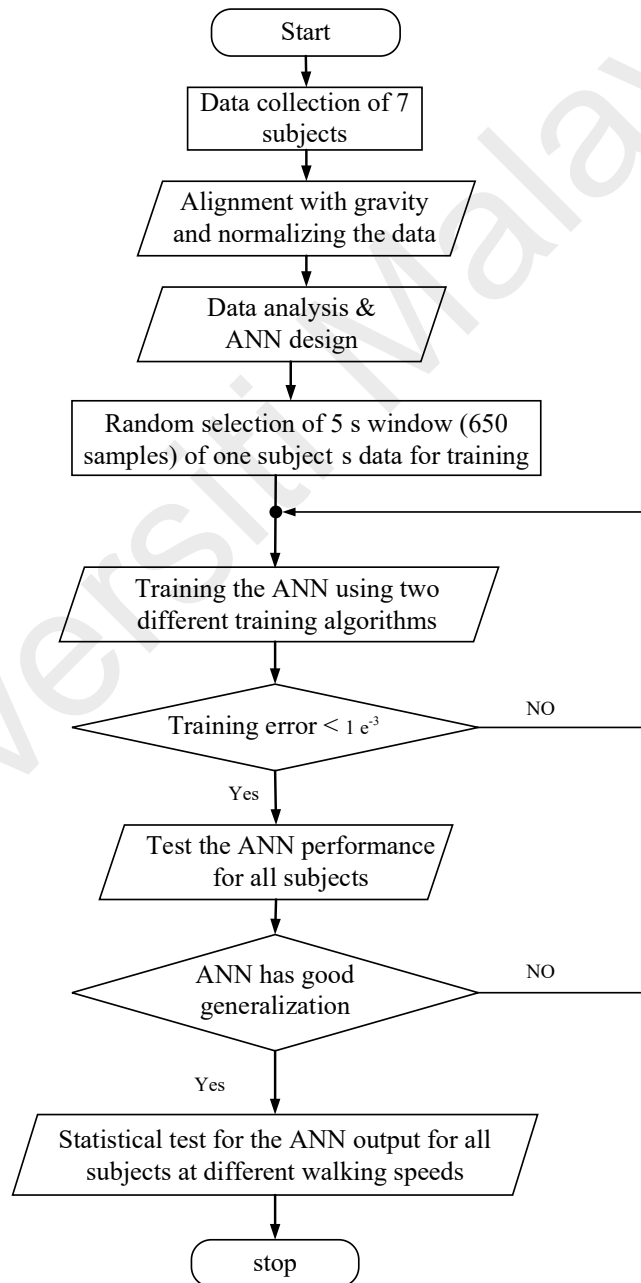
Figure 3.1: flowchart depicts the flow of the artificial neural network development in this study.

3.1 Experiment design and conduct

Seven healthy subjects participated in the experiment, one female (the sixth subject) and six males. Four OPAL wearable devices were attached to the lower limbs of each subject. OPAL is a miniature wearable and wireless IMU that can log and stream kinematic data in real time. The sensors were placed on the tibia and cuneiform bones in both right and left legs as shown in Figure 3.2. Each subject was instructed to walk on a treadmill for 12 min (To acquire huge data sets to test the efficiency of the neural network) at their own pace. Each subject walked the same trail again at two different speeds (±2% of the self-selected speed). The weight, height, self-selected speed, and experiment sequences are listed in Table 3.1. This study was approved by the Medical Research and Ethics Committee [reference number: KKM/NIHSEC/P19-2206(11)]. The sensor sample rate was 130 Hz. The data were transmitted in real time to a host computer where the raw data collected by the sensors were saved. Each subject performed three trials in one day. These trials were separated by an alignment procedure and recovery period as depicted in the pseudo code. Only the raw data of the three-axis accelerometer and the three-axis gyroscope of each OPAL sensor were used in this study.

Figure 3.2: A picture of the second subject shows the OPALs sensors placed on the tibia and cuneiform bones in both right and left legs.

Table 3.1: Information about the subjects and experiment sequences.

subjects	Weight (kg)	Height (cm)	Self-selected speed (normal) km/h	Sequence
S1	67	177	4.0	Day1 (Morning)
S2	80	167	4.0	Day1 (Afternoon)
S3	65	165	2.0	Day1 (Afternoon)
S4	84	180	2.0	Day2 (Morning)
S5	51	175	2.6	Day2 (Afternoon)
S6	48	166	3.5	Day2 (Afternoon)
S7	74	174	4.0	Day3 (Afternoon)
Average	67	172		

Pseudo code for normalization and alignment with gravity

Load Accelerometer Calibration Data   // subjects were asked to stand still for ten second for alignments

/* calculate the mean values of accelerometer data for three axes */

M_x = Mean (accelerometer data of the X axis)

M_y = Mean (accelerometer data of the Y axis)

M_z = Mean (accelerometer data of the Z axis)

/* data normalization */

M= [M_x M_y M_z]

Data = Data / norm (M)

/* calculate the rotation matrix*/

a= arctan (M_y / M_z)

b= arctan (-M_x / $\sqrt{My^2 + Mz^2}$)

c = arctan ($\sqrt{Mx^2 + My^2}$/ M_z)

Rotation Matrix =

$$\begin{bmatrix} \cos(b)*\cos(c) & -\cos(b)*\sin(c) & \sin(b) \\ \sin(a)*\sin(b)*\cos(c)+\cos(a)*\sin(c) & -\sin(a)*\sin(b)*\sin(c)+\cos(a)*\cos(c) & -\sin(a)*\cos(b) \\ -\cos(a)*\sin(b)*\cos(c)+\sin(a)*\sin(c) & \cos(a)*\sin(b)*\sin(c)+\sin(a)*\cos(c) & \cos(a)*\cos(b) \end{bmatrix}$$

/* calculate the aligned data*/

Aligned Gyroscope Data = Rotation Matrix^T * Gyroscope Data

Aligned Accelerometer Data = Rotation Matrix^T * Accelerometer Data

3.2 Data analysis & ANN design

Increasing evidence highlights a relationship between tibia kinematics and foot orientation during ambulation (Holgate et al., 2008; Holgate et al., 2009). Therefore, an ANN was developed based on this relationship to achieve the desired orientation of the prosthetic foot during ambulation with varying walking speeds. Embedding a 3-DOF gyroscope (or a 6-DOF IMU) to any robotic prosthesis is an easy task that does not affect the size or weight of the system (Li et al., 2013). Therefore, an IMU sensor can be mounted on a prosthetic leg to provide the angular velocity of the tibia as input to NARX RNN to generate a nonlinear foot pattern.

3.2.1　ANN input, output and structure

Human ambulation is complex and has highly coupled dynamics whose chaotic nature has been discussed in detail in many studies (Miller et al., 2006; Scafetta et al., 2009; West et al., 2003). (A. E. Martin et al., 2016) argued that the ankle joint has the largest variability oscillation among all joints in both swing and stance phases. Figure 3.3 (a) shows the quasiperiodic behavior between foot orientation and shank angular speed, whereas Figure 3.3 (b) illustrates the projection on the limit torus as defined by walking range of motion. An augmented Dickey–Fuller (ADF) t-statistic test was performed on the angular velocity of the tibia (used as input in the neural network), and results showed that such data are non-stationary time series with a unit root and a large p-value. Table 3.2 shows the p-values of the input signal of all subjects at different walking speeds. Furthermore, given that ankle control has a significant feedback loop (A. E. Martin et al., 2016), RNNs have a highly convenient structure for estimating foot orientation because of their superior non-stationary inputs (Galushkin, 2007).

The NARX neural network is among the most robust and commonly used techniques in predicting complex non-linear time series (Diaconescu, 2008; Menezes Jr et al., 2008).
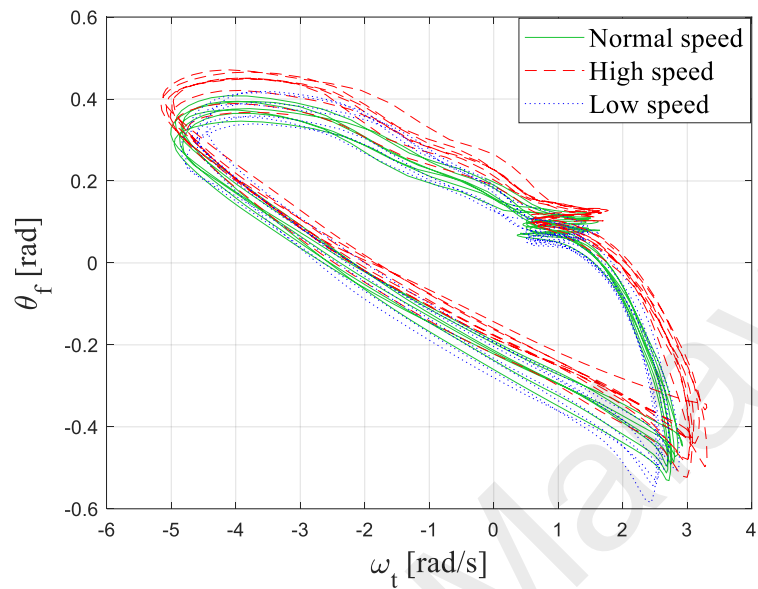
(a)
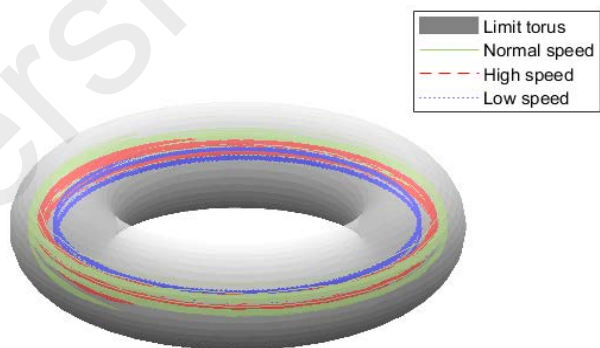
(b)

Figure 3.3: (a) The relation between shank angular speed and foot angular position in three different walking speeds. (b) The projection of angular speed and position on the limit torus. Where low, self-selected, and high speed are shown in blue, green, and red, respectively.

(Menezes Jr et al., 2008) found that NARX outperforms the topologies of other neural networks in estimating chaotic time series. NARX RNN is also suitable for generating non-linear oscillations associated with locomotion and is more convenient with long-term dependencies than conventional RNNs, where the embedded memory of the neural network helps accelerate the propagation of gradient information, thereby reducing the effect of vanishing gradient (Lin et al., 1996). NARX RNN also reduces the correlation among the input variables, which may degrade forecasting accuracy by interacting with one another and with other elements and producing a biased effect (Diaconescu, 2008; G. P. Zhang, 2004).

Table 3.2: The p-values resulted from Augmented Dickey–Fuller (ADF) t-statistic test of the tibia's angular velocity at different walking speeds (neural network input).

subjects	Walking speeds	p-values of the tibia's angular velocity
1	slow	0.3199
	normal	0.2860
	high	0.2657
2	slow	0.2665
	normal	0.2542
	high	0.1998
3	slow	0.5475
	normal	0.6443
	high	0.4215
4	slow	0.6135
	normal	0.7770
	high	0.4818
5	slow	0.3515
	normal	0.3029
	high	0.4113
6	slow	0.3281
	normal	0.3209
	high	0.4230
7	slow	0.1418
	normal	0.4799
	high	0.2124

One task of NARX is to filter the gyroscope low-frequency noise and integrate the input signal, which can be represented in the discrete time domain as shown in equation (1).

Following equation (1), the number of delays for the input and recurrent signal was set to 1 and 2, respectively.

$$y[k] = \frac{(2 + \omega_n \cdot T_s) \cdot y[k-1]}{1 + \omega_n \cdot T_s} - \frac{y[k-2]}{1 + \omega_n \cdot T_s} + \frac{T_s \cdot (u[k] - u[k-1])}{1 + \omega_n \cdot T_s} \qquad (1)$$

where y[k] is the normalized output of the neural network, u[k] is the angular speed of the tibia, and ω_n and Ts are the cut-off frequency and sample time of the filter, respectively.

The input signal (angular velocity of the shank) comprised five harmonics in the frequency domain as depicted in the single-sided amplitude spectrum of the fifth subject in Figure 3.4. The single-sided amplitude spectrum of the data for all participants are illustrated in Appendix A. Accordingly, the input feature space should be divided by five hypersurfaces (Galushkin, 2007). Five neurons in the first layer of the NARX RNN were initially chosen. After training the network, reducing the neurons in the first layer into four neurons had no effects on the training error. Meanwhile, in (Chinimilli, 2018) , only three harmonics were considered in the extraction of novel features for terrain and speed identification. However, further investigation is needed for slower speeds, where the fourth and fifth harmonics are more dominant.

The second layer task was to select the correct combination of regions. The maximum number of regions can be calculated using equation (2) (van den Berg, 2016), where *r(n,k),* k, and n denote the maximum number of regions, number of inputs, and number of neurons of the first layer, respectively. The maximum number of regions for the initial design was 16 ($\sum_{i=0}^{2} \binom{5}{i}$), which was reduced to 11 ($\sum_{i=0}^{2} \binom{4}{i}$) after decreasing the number of neurons of the first layer.

$$r(n,k) = \sum_{i=0}^{k} \binom{n}{i} \qquad (2)$$
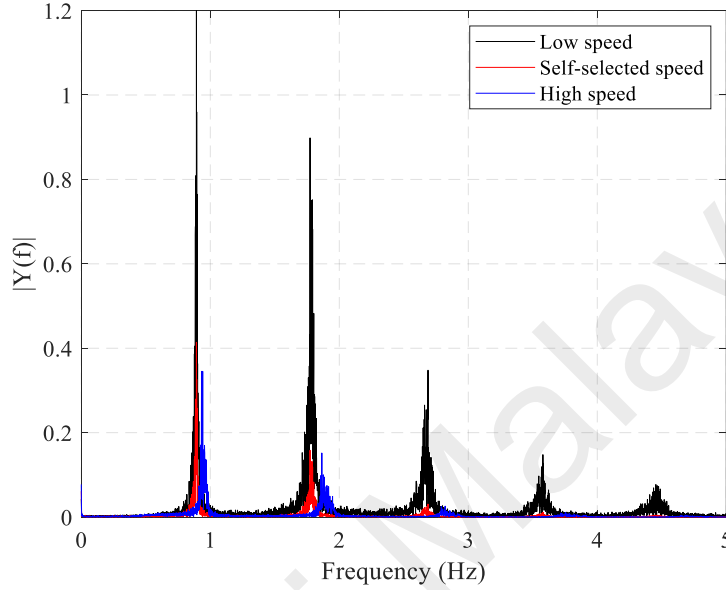
Figure 3.4: Single-sided amplitude spectrum of tibia angular speeds of the fifth subject.

The foot orientation as a function of tibia orientation (using a Fourier series) is given in equation (3). A total of 15 components are required from the series given in equation (3) to estimate foot orientation accurately. In equation (3), θ_{foot}, θ_{tibia}, a_0, a_n, and b_n represent the foot and shank orientations and the constant coefficients of the functions, respectively. Therefore, 15 neurons were selected for the second layer. Figure 3.5 shows the measured foot orientation and the foot orientation as a function of tibia orientation. The coefficients were calculated by fitting the non-linear least-squares curve.

$$\theta_{foot} = f(\theta_{tibia}) \cong \frac{a_0}{2} + \sum a_n \cdot \cos(n \cdot \theta_{tibia}) + \sum b_n \cdot \sin(n \cdot \theta_{tibia}) \qquad (3)$$
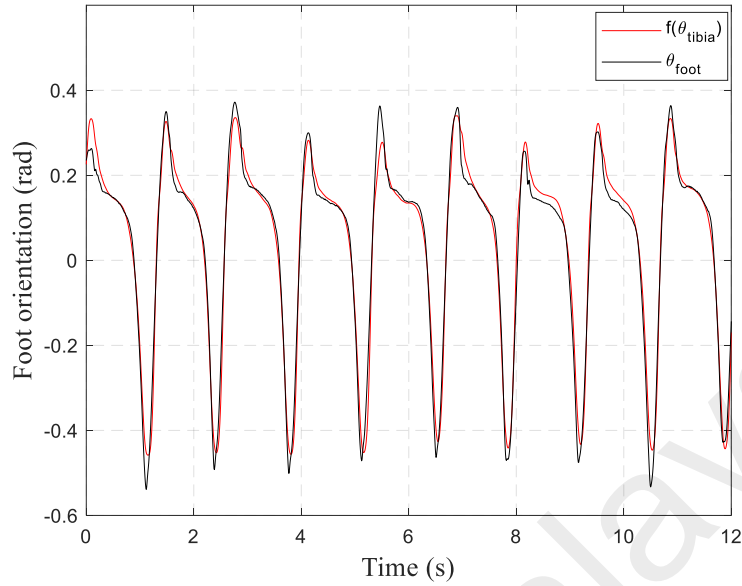
Figure 3.5: Foot orientation as a function of tibia orientation. Function and measured values are illustrated in solid red and black, respectively.

The proposed NARX network is shown in Figure 3.6, and the number of delays was chosen as previously discussed. After establishing the structure, the NARX RNN was ready for training.
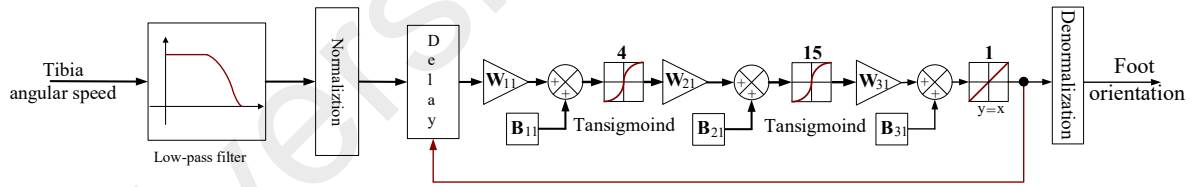
Figure 3.6: Block diagram of the proposed structure of the NARX network. The input data were filtered by low-pass filter, normalized, and aligned with gravity and local coordinate axis. The NARX RNN consist of two hidden layers. The first layer composed of four neurons and the second layer composed of fifteen neurons, each neuron has a hyperbolic tangent activation function. The activation function of the output layer is a pure line.

3.2.2   NARX training

The data of the third subject were randomly selected for the training procedure. A random selection was performed in line with the hypothesis of this work, that is, to design a user-independent pattern generator by having the NARX network learn the underlying relationship between the shank and foot. Moreover, as shown in section A of the Supplementary Material, all input data had a similar frequency spectrum. Therefore, a

38

combined training batch was not necessary. The output of the complementary filter (foot orientation in the sagittal plane) was selected as the target data, whereas the angular velocity of the shank was treated as the input data (Figure 3.7 shows the structure of the complementary filter). Only a 5 s window (650 samples) was selected for the training to avoid poor generalization, prevent degradation in accuracy, and achieve a faster empirical convergence (Kandel et al., 2020; Shallue et al., 2018; Yao et al., 2018). The training process was divided into two stages, namely, an open loop training where the target was fed instead of the recurrent signal and a close loop training where the recurrent signal was restored. Two training algorithms, namely, the Levenberg–Marquardt (LM) and Bayesian regularization (BR) backpropagations, were selected to train the NARX network. The LM algorithm is the fastest approach for training a mid-size feedforward ANN(Arora et al., 2016), whereas the BR method is highly robust against overfitting (Foresee et al., 1997).
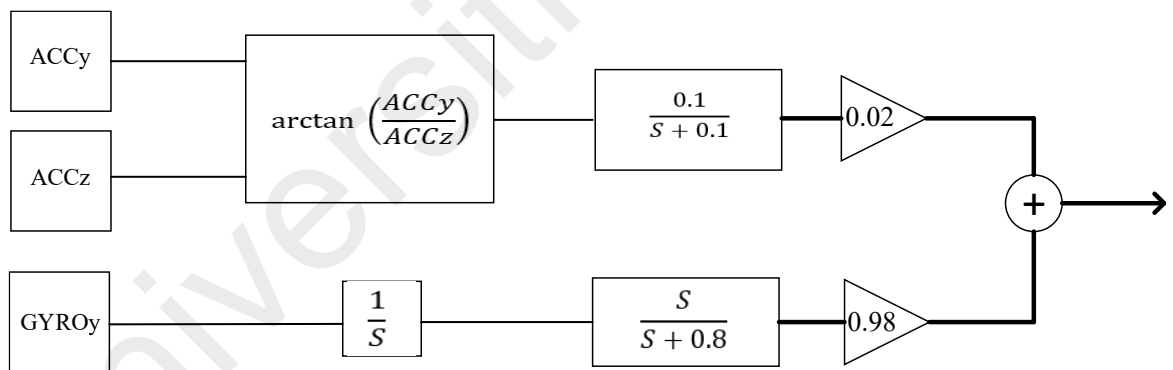
Figure 3.7: Block diagram of the used complementary

In line with (Foresee et al., 1997; Kayri, 2016), BR backpropagation outperformed LM with a training error of 1.1 e-08. After the training, NARX was assessed by using the data of all subjects at different walking speeds. The NARX RNN hyperparameters for the training algorithms are shown in Table 3.3.

Table 3.3: Training hyperparameters for LM and BR algorithms

Parameters	Value
LM algorithm	
Maximum number of epochs to train	75000
Performance goal	0
Marquardt adjustment parameter	0.005
Decrease factor for mu	0.1
Increase factor for mu	10
Maximum value for mu	1e10
Maximum validation failures	6
Minimum performance gradient	1e-18
BR algorithm	
Maximum number of epochs to train	75000
Performance goal	0
Marquardt adjustment parameter	0.005
Decrease factor for mu	0.4
Increase factor for mu	10
Maximum value for mu	1e10
Maximum validation failures	inf
Minimum performance gradient	1e-18

3.2.3   NARX testing

Several statistical tests were performed to evaluate estimation performance, and the estimated foot orientation was compared with the measured orientation. By using OPAL raw data, the orientation can be calculated based on a widely established method (complementary filter) (Oliveira et al., 1998; Tian et al., 2012). Precision and accuracy were evaluated using RMSE and mean absolute error (MAE), respectively. To check the ability of NARX to cancel the drift in gyroscope signals, the error signal (measured - estimation) was investigated by performing Student's t-test with a 5% significance level. If NARX can cancel the gyroscope drift, then the null hypothesis is supported (h=0). Furthermore, the cross-correlation was used

to illustrate the similarity between the estimations and measurements. The probabilistic consistency of the model and the histogram distribution of the measured and estimated signals were analyzed based on the extreme value distribution.

CHAPTER 4   RESULTS

The NARX network was built in MATLAB/Simulink (Figure 3.5), and the simulation model was run using the Euler fixed-step solver with a sampling rate of 130 Hz (sensor sampling rate). The data of all subjects were processed, and the estimated foot orientation was compared with the measured value. The overall size of the data was $7 \times 700 \times 3$ (denoting subjects, seconds, and speeds, respectively). All the data collected during the experiment were statistically analyzed.

4.1 Static and dynamic performance of the neural network

The mean values and standard deviations (SDs) of foot orientation (measured and estimated) in 100 consequent strides were compared for all subjects at different walking speeds (Figure 4.1). A new stride was detected through high-frequency noise, which occurs during a heel strike event. An adaptive window was constructed between every two heel strikes to determine the gait cycle. This procedure was terminated after covering 100 strides. The foot orientation of the fifth subject was selected for illustration. The results of the other subjects are listed in Appendix B.

Standard deviations show that the dynamic performance of NARX was comparable to that of the measured foot performance [Figures 4.1 (a), (b), and (c)]. The network encountered a problem with low-frequency changes, which appeared as static errors during the stance phase. The average RMSE for all subjects with different walking speeds was 2.1±1.7°. No explicit evidence indicates whether this range of error was within an acceptable threshold for practical implementation (Rai, Sharma, et al., 2019). Nonetheless, a low-level controller could be tuned to tolerate such static error.
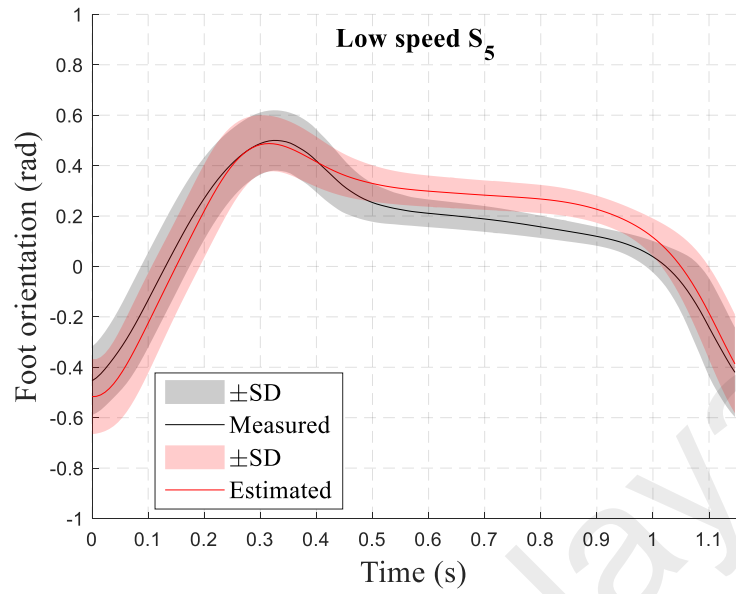
(a)
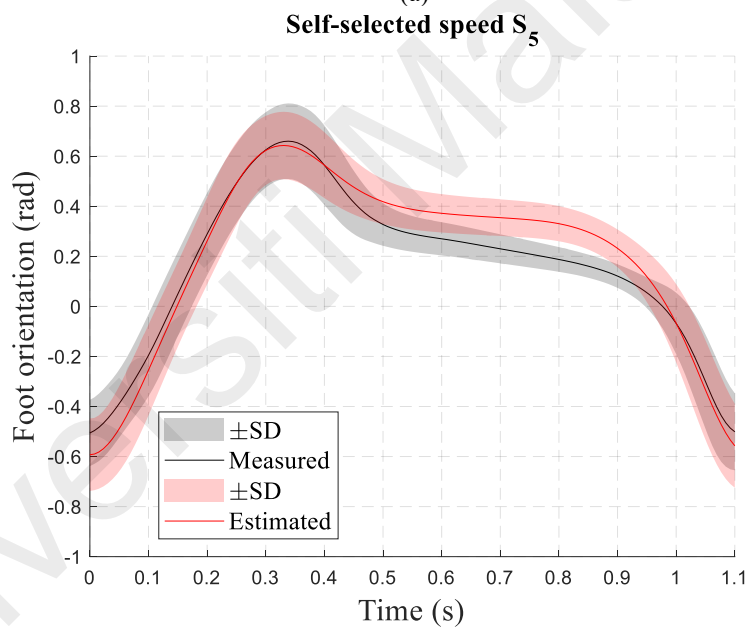
(b)
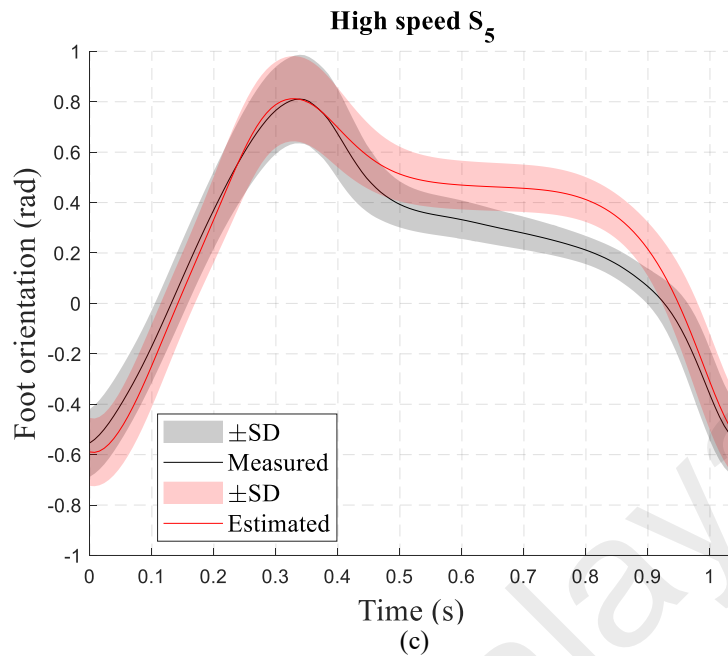
Figure 4.1: **Foot orientations at three different speeds of the fifth subject. The mean value of the estimated and measured orientation for 100 strides are presented in solid red and black, respectively. The standard deviations of the signals are illustrated in pink (estimated) and grey (measured).**

4.2 Probabilistic consistency of the model

The self-selected walking speed histogram and extreme value distribution (EVD) are illustrated in Figure 4.2. The EVDs of the measured and estimated signals were almost identical with a slight shift to the right (higher amplitude) for the distribution of the estimated value. This shift could be attributed to the static error in Figure 4 (a). The histograms and EVDs of all participants are shown in Appendix C.
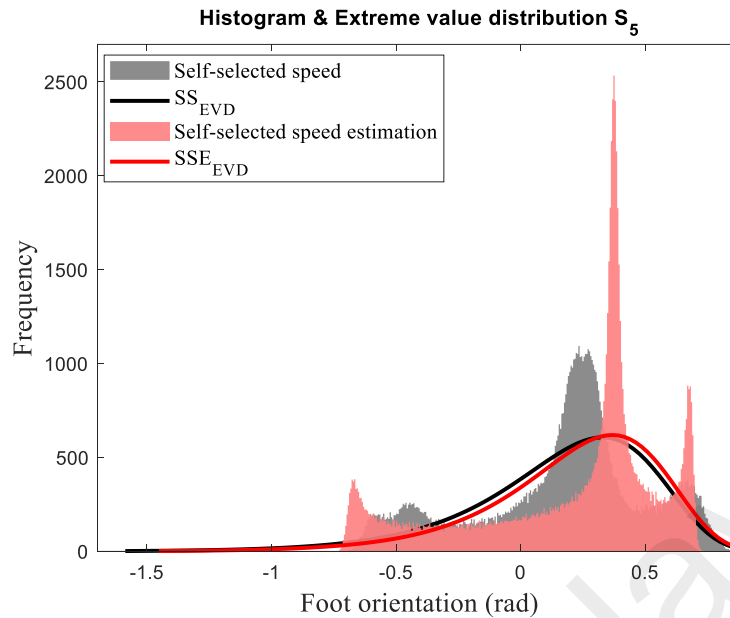
Figure 4.2: Foot orientation histogram and extreme value distribution. The distribution of estimated and measured values is shown in solid red and black, respectively. The histogram of the signals is shown in pink (estimated) and grey (measured).

4.3 Error range and distribution and the correlation between measured and estimated data

A statistical analysis of the network performance of all subjects in three different ambulation speeds was performed, and results are summarized in Table 4.1. The cross-correlation (r) value, RMSE, MAE, and t-test results for the error signals with all the critical values are shown in red.

The *r* values indicated similarities between the estimated and measured values. The minimum correlation was 86%, which was obtained at low-speed ambulation by the fourth subject. By contrast, all other *r* values exceeded 92%. *t*-test results showed that the error signals were normally distributed (central limit theorem) with a high certainty level (0.88 minimum p-value). The maximum RMSE and MAE in all trials were approximately 5° and 6°, respectively.

Table 4.1: Results of statistical analysis.

		Low speed	Normal speed	High speed
S1	r	0.96509	0.95098	0.96521
	RMSE	0.00905	0.00551	0.02182
	MAE	0.06350	0.09404	0.07685
	t-test[1]	m_e =-0.0091 p=1, h=0	m_e =-0.00551 p=0.9715, h=0	m_e =-0.0218 p=0.9310, h=0
S2	r	0.92214	0.94461	0.94661
	RMSE	0.01177	0.01370	0.00156
	MAE	0.10211	0.11533	0.10974
	t-test	m_e =0.0118 p=1, h=0	m_e =-0.0137 p=0.9987, h=0	m_e =0.0016 p=0.9425, h=0
S3	r	0.97997	0.98828	0.97734
	RMSE	0.02439	7.026e-04	0.00542
	MAE	0.06558	0.05251	0.05223
	t-test	m_e =-0.0244 p=1, h=0	m_e =-7.026e-04 p=1, h=0	m_e =-0.00542 p=1, h=0
S4	r	0.86499	0.92352	0.95316
	RMSE	0.09439	0.05965	0.03222
	MAE	0.10851	0.10339	0.09395
	t-test	m_e =-0.0944 p=0.9804, h=0	m_e =-0.0535 p=0.8964, h=0	m_e =-0.0322 p=0.9551, h=0
S5	r	0.96540	0.98037	0.97643
	RMSE	0.04733	0.02961	0.07488
	MAE	0.09294	0.08468	0.11540
	t-test	m_e =-0.0473 p=0.9243, h=0	m_e =-0.0296 p=0.9763, h=0	m_e =-0.0749 p=0.9731, h=0
S6	r	0.94919	0.94226	0.95069
	RMSE	0.07263	0.07263	0.07445
	MAE	0.07042	0.08619	0.08941
	t-test	m_e =-0.0582 p=0.9354, h=0	m_e =-0.0726 p=0.8807, h=0	m_e =-0.0745 p=0.9988, h=0
S7	r	0.96242	0.96482	0.95096
	RMSE	0.04775	0.00978	0.07416
	MAE	0.08149	0.06528	0.09612
	t-test	m_e =-0.0478 p=0.8777, h=0	m_e =0.0098 p=0.9515, h=0	m_e =-0.0742 p=0.8883, h=0

---

[1] T-test for the error vector (91001 samples)

CHAPTER 5 DISCUSSION

5.1 General discussion and research outline

This study aims to develop an adaptive and user-independent pattern generator toward constructing a unified controller for powered ankle prostheses. The proposed technique is inspired by the biological rhythmic signals generated by neural circuits distributed throughout the lower thoracic and lumbar regions of the spinal cord (Kiehn et al., 2003). To design and develop the neural network to achieve the required output signals and replace missing biological signals, three obligatory rules must be fulfilled to ensure the efficiency of a neural network and to estimate the desired output. These rules can also help overcome some problems associated with the training of neural networks, such as overfitting, poor generalization, and slow convergence (Wilamowski, 2009). These rules can be outlined as follows: 1) Choose a proper ANN architecture that fits the application. 2) Set the ANN size (number of layers and neurons at each layer). 3) Select the training algorithm that suits the neural network architecture and the data size and type.

First, for neural network selection, NARX RNN was used to generate the walking patterns. As described in Chapter 3, NARX was selected given its superior ability in predicting complex non-linear time series, its simple structure, and easy tuning. Moreover, given that the input data are non-stationary, an RNN structure is required considering its superiority over feedforward neural networks for a non-stationary input. NARX is also suitable for generating non-linear oscillations associated with locomotion and is more convenient for long-term dependencies than conventional RNNs.

Second, the NARX tasks were analyzed to set the NARX size, input, and delays of feedback signals. Following equation (1), the number of delays for the input and recurrent

signals was set to 1 and 2, respectively. The first layer comprised five neurons as defined by the results of a Fourier analysis of input signals comprising five harmonics. Reducing the number of neurons to four did not affect the training error. Using equation (3), the number of neurons for the second layer was set to 15. Selecting a proper size of the neural network (as minimal as possible) will facilitate the training procedure, reduce the overfitting possibilities, and improve generalization ability (Hunter et al., 2012).

Third, choosing the optimum training algorithm is more challenging and sophisticated than choosing the neural network architecture and its size. Given the countless training algorithms available in the literature and the lack of an optimum training method that suits all neural networks, the best training algorithm is subjective to the topology and size of the neural network and to the type and size of the training data (training samples). Tables 5.1 and 5.2 show the most commonly used first- and second-order training algorithms, respectively. Further details on these training algorithms can be found in (Ruder, 2016; Tan et al., 2019). Given the simple architecture of NARX RNN (which is neither a bridged multilayer perceptron BMLP nor a fully connected cascade FCC), the medium size of the designed neural network (i.e., 20 neurons), the small training data set, and the lack of any spare data, the LM and BR algorithms were chosen for training the neural networks. As depicted in Chapter 4, the BR algorithm outperformed LM with its lower training error and better generalization (check Table 3.3).

The resulting control system can respond to any user in a variety of walking speeds. The average RMSE for all subjects at different walking speeds was $2.1\pm1.7°$. No explicit evidence suggests whether this range of error is within an acceptable threshold for practical implementation (Rai, Sharma, et al., 2019). However, (Yuan et al., 2014) set the threshold of foot inclination angle at mid-stance for slopes detection to $\pm5°$, whereas (Sup et al., 2010) set

their threshold to ±2.5°. Therefore, the range of error of the pattern generator may not be noticed by users during its implementation. Nonetheless, such static error can be reduced by tuning the low-level controller of the overall control system. The standard deviations of the measured and the estimated data shows the accurate dynamic performance of the neural network. Also, statistical tests and the extreme values distribution of the data prove that the neural network's output has high similarity with the measured data and probabilistic consistency.

5.2 Comparison with the three-level conventional controllers

Similar to other methods inspired by neural circuits (Nandi et al., 2008; Rai & Rombokas, 2019; Rai, Sharma, et al., 2019), the proposed method aims to overcome the disadvantages of conventional three-level controllers. While these controllers are known for their non-dynamic switching rules, they are limited to few walking modes and cadences and cannot cover all types of slopes (i.e., different incline angles), stairs (i.e., variant heights and depths), and walking speeds.

The proposed algorithm can reduce the high computational load required for accurate mode recognition and processing multiple feedback signals. NARX RNN was deployed on TI's TMS320F28377S microcontroller and ran for 97.3 μs, thereby suggesting that this technique is implementable in real time.

Given that unilateral lower-limb amputees have average daily walking steps of 3063±1893 (Stepien et al., 2007), even a proportionally low classification error ranging from 1% to 2% can make the intermittent conventional controller misclassify 30 to 60 walking steps daily, hence exposing amputees to a high risk of falling. Moreover, although some errors may not directly expose amputees to falling risks, they can reduce their confidence in

using powered prosthetic devices (F. Zhang et al., 2012, 2014). Using the developed NARX dynamic pattern generator will eliminate the risks associated with classification errors.

5.3 Comparison with biological-signals-inspired controllers

The proposed method differs from other methods that are inspired by neuro-mechanical circuits. First, unlike the CPG-based method of (Nandi et al., 2008), the proposed method is user independent and does not require a specific design of the neural network for each user based on his/her height, weight, and age. This method can also be easily trained by a simple optimization algorithm. Second, in contrast to LSTM (Rai & Rombokas, 2019; Rai, Sharma, et al., 2019) the proposed method requires minimal sensory feedback, thereby increasing its acceptance among amputees, reducing the computational load, and minimizing the cost of prostheses. One 3-DOF gyroscope (or 6-DOF IMU) is enough to provide the neural network with the angular speed of the tibia to generate the missing foot trajectory throughout the ambulation. Moreover, the RMSE of the predicted ankle angle during ground-level walk was 4.4° and 4.23° in (Rai & Rombokas, 2019; Rai, Sharma, et al., 2019), respectively.

Table 5.1: First-order training algorithms.

Training algorithms	Update rules	Comments
Batch Gradient Descent (Curry, 1944)	$W_{new} = W_{old} + \eta \dfrac{\partial C}{\partial w}$ Where: W: weights vector or neural network parameters, some references use θ to refer to the network parameters. η : the learning rate, a constant value $0 \leq \eta \leq 1$. C: the cost function or the loss function or objective function based on the reference. There are many types of cost functions, but the most common and efficient cost function is the quadratic cost function, $C = \dfrac{1}{2} \sum_{j} (y_{desired} - y_{estimated})^2$	This method can be extremely slow, and it cannot update the system online. As the weights update happens only after a full epoch (training set), which causes this slow convergence.
Stochastic Gradient Descent (SGD)	$W_{t+1} = W_t + \eta \dfrac{\partial C}{\partial w}$ $C = \dfrac{1}{2} (y_{desired} - y_{estimated})^2$	In this method, the cost function is computed at each iteration (training sample) and the same for weights update. Unlike

(Kiefer et al., 1952).		Batch gradient Descent, where the cost function is based on the complete training set. This method is called stochastic, because the path towards the global cost minimum is not direct, but like zigzag if the cost surface is visualized in two-dimension. There are many types and updates to the SGD algorithm, and they vary with shuffling the samples before the training procedure.
Mini-Batch Gradient Descent (MB-GD) (Bottou et al., 2018;	$$W_{new} = W_{old} + \eta \frac{\partial C}{\partial w}$$ $$C = \frac{1}{2} \sum_k (y_{desired} - y_{estimated})^2$$	MB-GD is a compromise method between Batch gradient descent and SGD methods. Where, the weights will be updated every small batch or window of samples,

Robbins et al., 1951)		unlike SGD that updates the weights for every single sample or Batch gradient descent after full epoch.
SGD with momentum (Qian, 1999)	$\Delta w_t = \gamma \Delta w_{t-1} + \eta_t \dfrac{\partial C}{\partial w}$ $W_{t+1} = W_t - \Delta w_t$ Where: η_t: an adaptive learning rate, also in this method a constant learning rate can be used. γ: momentum term, usually set to 0.9. Δw_t: weights update vector.	The momentum will help to accelerate SGD towards the global minimal (faster convergence) and dampens the oscillations by the added fraction of the past update vector ($\gamma \Delta w_t$). The adaptive learning rate varies between studies, where there are plenty of updating rules for the learning rate in the literature.
Nesterov Accelerated Gradient (NAG)	$\widehat{W}_t = W_t - \gamma \Delta w_{t-1}$ $\Delta w_t = \gamma \Delta w_{t-1} + \eta_t \dfrac{\partial C}{\partial \widehat{W}_t}$ $W_{t+1} = W_t - \Delta w_t$	NAG method is an extension of momentum, instead of calculating the decaying moving average

(Nesterov, 1983)		of the actual gradients $\frac{\partial C}{\partial w}$ it will calculate the decaying moving average of the projected positions (an approximation of the next position) of network weights $\widehat{W_t}$. This technique can overcome some of the problems that could occur using SGD with momentum, such as missing or overshoot the minimal at the bottom of the basins. Also, it is faster.
Adaptive Gradient Algorithm (Adagrad) (Duchi et al., 2011)	$g_{t,i} = \frac{\partial C_{t,i}}{\partial w_{t,i}}$ $W_{t+1,i} = W_{t,i} - \frac{\eta_t}{\sqrt{G_{t,ii} + \epsilon}} \cdot g_{t,i}$ Where: $g_{t,i}$: is the partial derivative of the cost function with respect to the weight $w_{t,i}$, the gradient at time step t.	In Adagrad the adaptive learning will update each weight independently, where the weights associated with frequent occurring features will have smaller updates. While for the weights associated with

$G_{t,ii}$: is a diagonal matrix, where each diagonal element ii is the sum of the squared gradients. ϵ: is a smoothing term to avoid the division by zero, usually $\epsilon = 1e^{-8}$.	infrequent occurring features will larger updates. Adagrad has significantly improved the SGD performance and eliminates the need to tune the value of the learning rate manually (it set mostly while using Adagrad at 0.1). However, this method accumulates the squared gradients in the denominator. Which will keep growing during the training procedure, thus the update vector will keep shrinking until it becomes infinitesimal. Consequently, the algorithm will be no longer able to update the weights.

Adadelta (Zeiler, 2012)	$E\lvert g_t^2\rvert_t = \rho E\lvert g_t^2\rvert_{t-1} + (1-\rho)g_t^2$ $RMS[g]_t = \sqrt{E\lvert g_t^2\rvert_t + \epsilon}$ $\Delta w_t = -\dfrac{\eta}{RMS[g]_t}\,g_t$ $W_{t+1} = W_t + \Delta w_t$ Also, authors suggested a replacement of η with $RMS[\Delta w]_{t-1}$. $RMS[\Delta w]_{t-1} = \sqrt{E\lvert \Delta w_{t-1}^2\rvert_t + \epsilon}$ $E\lvert \Delta w_{t-1}^2\rvert_t = \rho E\lvert \Delta w_{t-1}^2\rvert_{t-1} + (1-\rho)\Delta w_{t-1}^2$	This method is an extension of the Adagrad method. In Adadelta the accumulation of the squared gradients is exponentially decaying average, which makes Adadelta overcomes the continuous decaying of the update vector associated with the Adagrad method.
Adaptive Moment Estimation (Adam) (Kingma et al., 2014)	$m_t = \beta_1 m_{t-1} + (1-\beta_1)g_t$ $v_t = \beta_2 v_{t-1} + (1-\beta_2)g_t^2$ β_1, β_2: constants set close to 1. $\widehat{m_t} = \dfrac{m_t}{(1-\beta_1^{\,t})}$ $\widehat{v_t} = \dfrac{v_t}{(1-\beta_2^{\,t})}$ $\Delta w_t = -\dfrac{\eta}{\sqrt{\widehat{v_t}}+\epsilon}\,\widehat{m_t}$ $W_{t+1} = W_t + \Delta w_t$ Also, authors suggested an alternative to η : $\alpha_t = \alpha.\dfrac{\sqrt{1-\beta_2^{\,t}}}{(1-\beta_1^{\,t})}$	This method was developed to combine the advantages of both Adagrad and RMSProp (can be seen as a special case of Adadelta). Adam works grate with spare gradients like Adagrad and works well online and with non-stationary data.

AdaMax (Kingma et al., 2014)	$u_t = \max(\beta_2 u_{t-1}, \lvert g_t \rvert)$ $\Delta w_t = -\dfrac{\eta}{u_t}\widehat{m_t}$ Or $\Delta w_t = -\dfrac{\alpha}{1-{\beta_1}^t}\cdot\dfrac{\widehat{m_t}}{u_t}$ $W_{t+1} = W_t + \Delta w_t$	This method is developed at the same paper with Adam. Instead of scaling the gradients by the squared norm L^2 during the current and past training step, authors used the infinite norm L^∞. Using the infinite norm, v_t converges to the more stable value.
Nesterov Accelerated Adaptive Moment Estimation (Nadam) (Dozat, 2016)	$\Delta w_t = -\dfrac{\eta}{\sqrt{\widehat{v_t}}+\epsilon}\left(\beta_1\widehat{m_t}+\dfrac{(1-\beta_1)g_t}{1-{\beta_1}^t}\right)$ $W_{t+1} = W_t + \Delta w_t$	Authors stated that the suggested method improves the speed of convergence and the quality of the learned models.
AdamW (Loshchilov et al., 2017)	$\Delta w_t = -\eta\left(\dfrac{\widehat{m_t}}{\sqrt{\widehat{v_t}}+\epsilon}+\gamma w_t\right)$ $W_{t+1} = W_t + \Delta w_t$	In this method, the weight decay technique is implemented. But the

		implementation was on the update vector rather than weights gradients. This method shows better generalization in practice.
AMSGRAD (Reddi et al., 2019)	$$\hat{v}_t = \max(\widehat{v_{t-1}}, v_t)$$ $$\Delta w_t = -\frac{\eta}{\sqrt{\hat{v}_t} + \epsilon} m_t$$ $$W_{t+1} = W_t + \Delta w_t$$	In some cases, the adaptive learning algorithms (Adadelta, Adam, Adamax, Nadam) are outperformed by SGD. Authors stated that the problem of the poor generalization is due to the exponential moving average of past squared gradients. Therefore, they proposed their method to overcome this problem. authors observed improve performance with small datasets. However, the method showed similar or worse performance in other experiments.

Quasi-Hyperbolic Adam (QHAdam) (Ma et al., 2018)	$\Delta w_t = -\eta \left[\dfrac{(1 - v_1)g_t + v_1\widehat{m_t}}{\sqrt{(1 - v_2)g_t^2 + v_2\widehat{v_t}} + \epsilon} \right]$ v_1, v_2: are immediate discount factors. $W_{t+1} = W_t + \Delta w_t$	This algorithm leads to significantly improved training in a variety of settings. Also, it can be seen as a general formula of Adam and Nadam algorithms, where the quasi-hyperbolic formulation is capable of recovering Adam and NAdam.
Aggregated Momentum (AggMo) (Lucas et al., 2018)	$V_t^{(i)} = \beta^{(i)}.V_{t-1}^{(i)} + g_t$ $W_t = W_{t-1} - \eta_t \left[\dfrac{1}{k} \sum_{i=1}^{k} V_t^{(i)} \right]$ $\beta = 1 - \alpha^{i-1}$ Authors suggested k=3, and α= 0.1 as good default choice.	This method is one of gradient momentum methods, which combines multiple velocity vectors with different scaling parameters. AggMo is easy to implement, and it significantly dampens oscillations, which makes it stable even with a high β value. This method can

		be seen as a general formula of Nesterov.

Table 5.2: Second-order training algorithms.

Training algorithms	Update rules	Comments
Newton's method (Nocedal et al., 2006)	$W_{t+1} = W_t - \eta\left(H_t^{-1} \cdot g_t\right)$ g_t: is the gradient vector, the first order derivatives of the cost function (loss function) with respect to the weight $w_{t,i}$. $g_{t,i} = \frac{\partial C_t}{\partial w_{t,i}}$ H_t: is the Hessian matrix, the second order derivatives of the loss function with respect to the weights $w_{t,i}$, $w_{t,j}$. $H_{t,i,j} = \frac{\partial^2 C_t}{\partial w_{t,i} \partial w_{t,j}}$	Although Newton's method requires fewer steps to converge compared with first-order methods, it is highly computationally expensive. Where, it needs to compute the Hessian matrix and its inverse.
Conjugate gradient method (Møller, 1993)	$d_0 = g_0$ $d_{t+1} = g_{t+1} + \gamma_t d_t$ $W_{t+1} = W_t + \eta_t d_t$ γ_t: is the conjugate parameter, there are different ways to calculate it. Two of the most used	This method can be regarded as something intermediate between gradient descent and Newton's method. It is so similar to SGD with

	are by Fletcher and Reeves (Fletcher et al., 1964) and Polak and Ribiere (Polak et al., 1969).	momentum or any adaptive first order method.
Quasi-Newton method (Robitaille et al., 1970)	$$W_{t+1} = W_t - \eta(G_t . g_t)$$ Where: G_t using DFP formula is given by the following equation. $$G_t = G_{t-1} - \frac{G_t y_t y_t^T G_t}{y_t^T G_t y_t} + \frac{s_t s_t^T}{s_t^T y_t}$$ Or using BFGS formula. $$G_t = G_{t-1} + \frac{(s_t y_t + y_t^T G_t y_t) s_t s_t^T}{(s_t^T y_t)^2}$$ $$- \frac{G_t y_t s_t^T + s_t y_t^T G_t}{s_t^T y_t}$$ $$s_t = W_t - W_{t-1}$$ $$y_t = g_t - g_{t-1}$$	This method uses inverse Hessian estimation to compute each update iteration. There are two famous methods to compute the estimated Hessian. First, Davidon-Fletcher-Powell (DFP) method. Second, Broyden-Fletcher-Goldfard-Shanno method (BFGS). This method is fasted than Newton's method and it is not computationally expensive.
Levenberg-Marquardt (LM) method (Roweis, 1996)	$$J_t = \frac{\partial e_t}{\partial w_{j,i}}$$ $$H = J_t^T . J_t + \mu I$$	This method is extremely fast, easy to implement, and it is

	$$W_{t+1} = W_t - \left(J_t^T . J_t + \mu I\right)^{-1} J_t e_t$$ J_t: Jacobian matrix e_t: is the error μ: is the combination coefficient I: is the identity matrix	inexpensive. Those properties make this method one of the most used training algorithms in the literature. However, this algorithm has some drawbacks. The first one is that it cannot be applied to functions such as the root mean squared error or the cross-entropy error. Also, for big data sets and neural networks, the Jacobian matrix becomes enormous, and therefore it requires much memory. Therefore, the Levenberg-Marquardt algorithm is not recommended when it

		is required to train a big neural networks or have huge data sets.
Neuron By Neuron (NBN) method (Wilamowski et al., 2018)	To compute the Jacobian matrix, the following three steps must be proceeded: 1. Forward computation: the selected computing sequence has to follow the concept of feedforward signal propagation, the following two temporary vectors are stored: the first vector y with the values of the signals on the neuron output nodes and the second vector s with the values of the slopes of the neuron activation functions, which are signal-dependent. 2. Backward computation: the selected computing sequence has to follow the concept of backpropagation. The vector δ will be stored, which represents signal propagation from	The NBN algorithm is developed for training arbitrarily connected neural networks (bridged multilayer perceptron BMLP, and fully connected cascade FCC). NBN algorithm only differ from LM algorithm by Jacobian matrix calculation.

	a network output to the inputs of all other neurons. The size of this vector is equal to the number of neurons. 3. Jacobian element computation: $$J_t = \frac{\partial e_t}{\partial w_{j,i}} = y_{j,i}.\delta_{t,j}$$ $$H = {J_t}^T.J_t + \mu I$$ $$W_{t+1} = W_t - \left({J_t}^T.J_t + \mu I\right)^{-1} J_t e_t$$	
Bayesian regularization (BR) method (Foresee et al., 1997)	$$F = \beta_t E_D + \alpha_t E_w$$ Where: E_D: is the sum of network errors. E_w: is the sum of the squared network weights. α_t, β_t: the objective function (loss or cost function) parameters. $$\alpha_t = \frac{\gamma}{2E_w}, \beta_t = \frac{n-\gamma}{2E_D}$$ γ: is the effective number of parameters. $$\gamma = N - 2\alpha_{t-1}.tr(H^{-1})$$ N: is the total number of weights. $$H = {J_t}^T.J_t + \mu I$$ $$W_{t+1} = W_t - \left({J_t}^T.J_t + \mu I\right)^{-1} J_t e_t$$	Bayesian regularization differs from LM algorithm by the cost function, where the optimum α_t, β_t will lead to better generalization and avoid overfitting.

CHAPTER 6 CONCLUSION

One challenge that must be addressed in developing powered prosthetic devices is their ability to generate human-like walking trajectories over different and irregular terrains. In this study, a NARX RNN was developed to estimate foot orientation from the angular velocity of the tibia as measured by IMU. To achieve the first objective the NARX RNN was constructed based on mathematical and statistical approaches. Moreover, to verify the fulfillment of the second objective, the experimental results were analysed statistically to ascertain the NARX RNN ability to generalize the results of all subjects at different walking speeds. The NARX RNN was able to generate foot trajectories for 7 subjects at different walking speeds over flat terrains with an average RMSE of $2.1\pm1.7°$. Consequently, it can perform similar to the neuro-mechanical circuit and give the right command (walking patterns) to lower-level controllers to control the prosthetic foot and makes it act similar to the biological foot.

6.1 Study limitation

1. The developed neural network has not been tested over variant terrains.
2. The neural network must be combined with low level controllers to imitate the intact foot behavior throughout the walking phases.

6.2 Future work

The human locomotion control strategy, which controls human locomotion, is not a form of a classic position controller. Consequently, it does not drive the body joints just to reach predetermined kinematics (Ahn et al., 2012). Moreover, the environment has inertias and kinematic constraints that are described as admittance. Therefore, prosthetic devices should behave as spring-damper systems with adaptive impedance, which should be modulated

along the gait cycle to regulate the dynamic interaction between the environment and prostheses and to generate a disturbance response for ensuring physical compatibility (Hogan, 1985). Thus, in future work, the output of the neural network should be transmitted to a mid-level controller that determines the ankle prosthesis control behavior during walking phases (Al Kouzbary et al., 2020). Moreover, the hierarchical three-level controller should be tested over different walking terrains (Figure 6 shows the complete control structure of the powered ankle prostheses).

6.3 Novelty of the study

1. The proposed pattern generator can provide continuous and dynamic control signals to the mid-level control system of prostheses in contrast to conventional three-level strategies in which the trajectory is predetermined.

2. The proposed technique does not require retraining for each user (i.e., user independent) and can generate the appropriate foot trajectory for different walking speeds (adaptive to varying cadences).

3. In contrast to existing controllers inspired by central biological signals, the proposed technique requires minimal feedback signals.
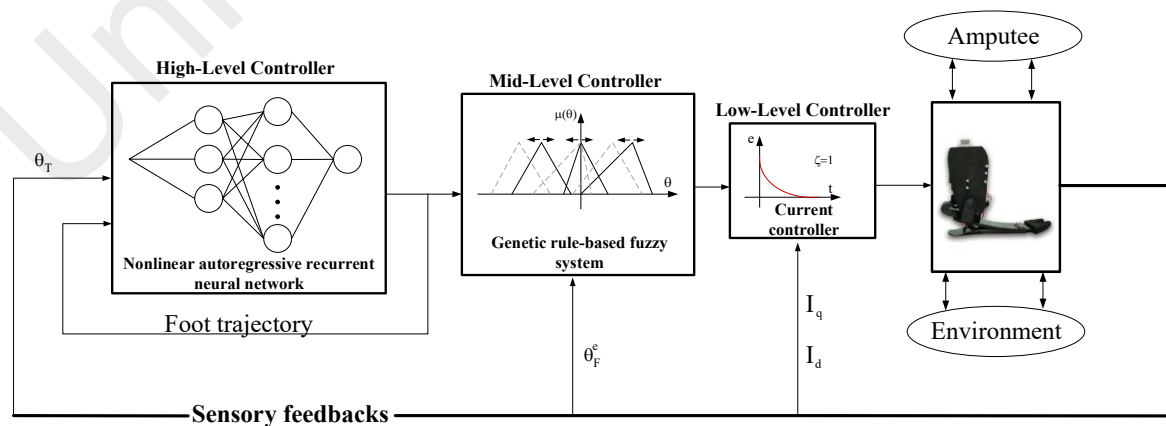

Figure 6.1: Continuous hierarchical control system.

REFERENCES

Ahn, J., & Hogan, N. (2012). Walking Is Not Like Reaching: Evidence from Periodic Mechanical Perturbations. *PLoS ONE*, 7(3), e31767.

Al Kouzbary, M., Abu Osman, N. A., Al Kouzbary, H., Shasmin, H. N., & Arifin, N. (2020). Towards Universal Control System for Powered Ankle–Foot Prosthesis: A Simulation Study. *International Journal of Fuzzy Systems*, , 22(4), 1299-1313.

Arora, I., & Saha, A. (2016). *Comparison of Back Propagation Training Algorithms for Software Defect Prediction.* Paper presented at the 2016 2nd International Conference on Contemporary Computing and Informatics (IC3I).

Au, S., Berniker, M., & Herr, H. (2008). Powered Ankle-Foot Prosthesis to Assist Level-Ground and Stair-Descent Gaits. *Neural Networks, 21*(4), 654-666.

Au, S. K., Bonato, P., & Herr, H. (2005). *An EMG-Position Controlled System for an Active Ankle-Foot Prosthesis: An Initial Experimental Study.* Paper presented at the 9th International Conference on Rehabilitation Robotics, 2005. ICORR 2005.

Au, S. K., Herr, H., Weber, J., & Martinez-Villalpando, E. C. (2007). *Powered Ankle-Foot Prosthesis for The Improvement of Amputee Ambulation.* Paper presented at the 2007 29th annual international conference of the IEEE engineering in medicine and biology society.

Behel, J. M., Rybarczyk, B., Elliott, T. R., Nicholas, J. J., & Nyenhuis, D. (2002). The Role of Perceived Vulnerability in Adjustment to Lower Extremity Amputation: A Preliminary Investigation. *Rehabilitation Psychology, 47*(1), 92–105.

Bottou, L., Curtis, F. E., & Nocedal, J. (2018). Optimization Methods for Large-Scale Machine Learning. *Siam Review, 60*(2), 223-311.

Burke, M., Roman, V., & Wright, V. (1978). Bone and Joint Changes in Lower Limb Amputees. *Annals of the rheumatic diseases, 37*(3), 252-254.

Chen, B., Zheng, E., Fan, X., Liang, T., Wang, Q., Wei, K., & Wang, L. (2013). Locomotion Mode Classification Using a Wearable Capacitive Sensing System. *IEEE transactions on neural systems and rehabilitation engineering, 21*(5), 744-755.

Cherelle, P., Junius, K., Grosu, V., Cuypers, H., Vanderborght, B., & Lefeber, D. (2014). The amp-foot 2.1: Actuator Design, Control and Experiments with an Amputee. *Robotica, 32*(8), 1347-1361.

Chevallereau, C., Grizzle, J. W., & Shih, C.-L. (2010). Asymptotically Stable Walking of a Five-Link Underactuated 3D Bipedal Robot. *arXiv preprint arXiv:1002.3258*.

Chevallereau, C., Westervelt, E., & Grizzle, J. (2005). Asymptotically Stable Running for a Five-Link, Four-Actuator, Planar Bipedal Robot. *The International Journal of Robotics Research, 24*(6), 431-464.

Chinimilli, P. T. (2018). *Human Activity Recognition and Control of Wearable Robots.* Arizona State University.

Curry, H. B. (1944). The Method of Steepest Descent for Non-linear Minimization Problems. *Quarterly of Applied Mathematics, 2*(3), 258-261.

Di Canio, G., Larsen, J. C., Wörgötter, F., & Manoonpong, P. (2016). *A Combination of Central Pattern Generator-Based and Reflex-Based Neural Networks for Dynamic, Adaptive, Robust Bipedal Locomotion.* Paper presented at the 1st International Symposium on Swarm Behavior and Bio-Inspired Robotics.

Diaconescu, E. (2008). The Use of NARX Neural Networks to Predict Chaotic Time Series. *Wseas Transactions on computer research, 3*(3), 182-191.

Dozat, T. (2016). Incorporating Nesterov Momentum into Adam. ICLR Workshop, (1):2013–2016.

Duchi, J., Hazan, E., & Singer, Y. (2011). Adaptive Subgradient Methods for Online Learning and Stochastic Optimization. *Journal of machine learning research, 12*(7), 2121-2159.

Ephraim, P. L., Wegener, S. T., MacKenzie, E. J., Dillingham, T. R., & Pezzin, L. E. (2005). Phantom Pain, Residual Limb Pain, and Back Pain in Amputees: Results of A National Survey. *Archives of physical medicine and rehabilitation, 86*(10), 1910-1919.

Farry, K. A., Walker, I. D., & Baraniuk, R. G. (1996). Myoelectric Teleoperation of a Complex Robotic Hand. *IEEE Transactions on Robotics and Automation, 12*(5), 775-788.

Ficanha, E. M., Rastgaar, M., & Kaufman, K. R. (2015). *Control of a 2-DOF Powered Ankle-Foot Mechanism.* Paper presented at the 2015 IEEE International Conference on Robotics and Automation (ICRA).

Fletcher, R., & Reeves, C. M. (1964). Function Minimization by Conjugate Gradients. *The computer journal, 7*(2), 149-154.

Flowers, W. C., & Mann, R. W. (1977). An Electrohydraulic Knee-Torque Controller for a Prosthesis Simulator. *Journal of Biomechanical Engineering*, 99(1), 3-8.

Foresee, F. D., & Hagan, M. T. (1997). *Gauss-Newton approximation to Bayesian learning.* Paper presented at the Proceedings of international conference on neural networks (ICNN'97).

Galushkin, A. I. (2007). *Neural Networks Theory*: Springer Science & Business Media.

68

Gao, F., Liu, Y., & Liao, W.-H. (2019). Implementation and Testing of Ankle-Foot Prosthesis with a New Compensated Controller. *IEEE/ASME Transactions on Mechatronics, 24*(4), 1775-1784.

Goldfarb, M., Lawson, B. E., & Shultz, A. H. (2013). Realizing The Promise of Robotic Leg Prostheses. *Science translational medicine, 5*(210), 210ps215-210ps215.

Grasso, R., Ivanenko, Y. P., Zago, M., Molinari, M., Scivoletto, G., Castellano, V., Macellari, V., & Lacquaniti, F. (2004). Distributed Plasticity of Locomotor Pattern Generators in Spinal Cord Injured Patients. *Brain, 127*(5), 1019-1034.

Gregg, R. D., Lenzi, T., Hargrove, L. J., & Sensinger, J. W. (2014). Virtual Constraint Control of a Powered Prosthetic Leg: From Simulation to Experiments with Transfemoral Amputees. *IEEE Transactions on Robotics, 30*(6), 1455-1471.

Grimes, D., Flowers, W. C., & Donath, M. (1977). Feasibility of an Active Control Scheme for Above Knee Prostheses. *Journal of Biomechanical Engineering*, 99(4), 215-221.

Hargrove, L., Huang, H., Schultz, A., Lock, B., Lipschutz, R., & Kuiken, T. (2009). *Toward The Development of a Neural Interface for Lower Limb Prosthesis Control.* Paper presented at the 2009 Annual International Conference of the IEEE Engineering in Medicine and Biology Society.

Hogan, N. (1985). Impedance control: An approach to manipulation: Part II—Implementation. *Journal of Dynamic Systems, Measurement,* and Control, 107(1), 8–16.

Holgate, M. A., Bohler, A. W., & Suga, T. G. (2008). *Control Algorithms for Ankle Robots: A Reflection on the State-of-The-Art and Presentation of Two Novel Algorithms.* Paper presented at the 2008 2nd IEEE RAS & EMBS international conference on biomedical robotics and biomechatronics.

Holgate, M. A., Sugar, T. G., & Bohler, A. W. (2009). *A Novel Control Algorithm for Wearable Robotics Using Phase Plane Invariants.* Paper presented at the 2009 IEEE International Conference on Robotics and Automation.

Horgan, O., & MacLachlan, M. (2004). Psychosocial Adjustment to Lower-Limb Amputation: a review. *Disability and rehabilitation, 26*(14-15), 837-850.

Huang, H., Kuiken, T. A., & Lipschutz, R. D. (2008). A Strategy for Identifying Locomotion Modes Using Surface Electromyography. *IEEE Transactions on Biomedical Engineering, 56*(1), 65-73.

Huang, H., Zhang, F., Hargrove, L. J., Dou, Z., Rogers, D. R., & Englehart, K. B. (2011). Continuous Locomotion-Mode Identification for Prosthetic Legs Based on Neuromuscular–Mechanical Fusion. *IEEE Transactions on Biomedical Engineering, 58*(10), 2867-2875.

Hunter, D., Yu, H., Pukish III, M. S., Kolbusz, J., & Wilamowski, B. M. (2012). Selection of Proper Neural Network Sizes and Architectures—A Comparative Study. *IEEE Transactions on Industrial Informatics, 8*(2), 228-240.

Inada, H., & Ishii, K. (2003). *Behavior Generation of Bipedal Robot Using Central Pattern Generator (CPG)(1st report: CPG Parameters Searching Method by Genetic Algorithm).* Paper presented at the Proceedings 2003 IEEE/RSJ International Conference on Intelligent Robots and Systems (IROS 2003)(Cat. No. 03CH37453).

Jimenez-Fabian, R., & Verlinden, O. (2012). Review of Control Algorithms for Robotic Ankle Systems in Lower-Limb Orthoses, Prostheses, and Exoskeletons. *Medical engineering & physics, 34*(4), 397-408.

Jones, L., Hall, M., & Schuld, W. (1993). Ability or Disability? A Study of The Functional Outcome of 65 Consecutive Lower Limb Amputees Treated at the Royal South Sydney Hospital in 1988-1989. *Disability and rehabilitation, 15*(4), 184-188.

Kandel, I., & Castelli, M. (2020). The Effect of Batch Size on The Generalizability of The Convolutional Neural Networks on a Histopathology Dataset. *ICT Express*, 6(4), 312-315.

Kayri, M. (2016). Predictive Abilities of Bayesian Regularization and Levenberg–Marquardt Algorithms in Artificial Neural Networks: A Comparative Empirical Study on Social Data. *Mathematical and Computational Applications, 21*(2), 20.

Kiefer, J., & Wolfowitz, J. (1952). Stochastic Estimation of The Maximum of a Regression Function. *The Annals of Mathematical Statistics*, 23(3), 462-466.

Kiehn, O., & Butt, S. J. (2003). Physiological, Anatomical and Genetic Identification of CPG Neurons in The Developing Mammalian Spinal Cord. *Progress in neurobiology, 70*(4), 347-361.

Kingma, D. P., & Ba, J. (2014). Adam: A Method for Stochastic Optimization. *arXiv preprint arXiv:1412.6980*.

Lawson, B. E., Varol, H. A., Huff, A., Erdemir, E., & Goldfarb, M. (2012). Control of Stair Ascent and Descent with a Powered Transfemoral Prosthesis. *IEEE transactions on neural systems and rehabilitation engineering, 21*(3), 466-473.

Lemaire, E. D., & Fisher, F. R. (1994). Osteoarthritis and Elderly Amputee Gait. *Archives of physical medicine and rehabilitation, 75*(10), 1094-1099.

Li, Y. D., & Hsiao-Wecksler, E. T. (2013). *Gait Mode Recognition and Control for a Portable-Powered Ankle-Foot Orthosis.* Paper presented at the 2013 IEEE 13th International Conference on Rehabilitation Robotics (ICORR).

Lin, T., Horne, B. G., Tino, P., & Giles, C. L. (1996). Learning Long-Term Dependencies in NARX Recurrent Neural Networks. *IEEE Transactions on Neural Networks, 7*(6), 1329-1338.

Liu, M., Wang, D., & Huang, H. H. (2015). Development of an Environment-Aware Locomotion Mode Recognition System for Powered Lower Limb Prostheses. *IEEE transactions on neural systems and rehabilitation engineering, 24*(4), 434-443.

Loshchilov, I., & Hutter, F. (2017). Decoupled Weight Decay Regularization. *arXiv preprint arXiv:1711.05101*.

Lucas, J., Sun, S., Zemel, R., & Grosse, R. (2018). Aggregated Momentum: Stability Through Passive Damping. *arXiv preprint arXiv:1804.00325*.

Ma, J., & Yarats, D. (2018). Quasi-Hyperbolic Momentum and Adam for Deep Learning. *arXiv preprint arXiv:1810.06801*.

Martin, A. E., & Gregg, R. D. (2015). *Hybrid Invariance and Stability of a Feedback Linearizing Controller for Powered Prostheses.* Paper presented at the 2015 American Control Conference (ACC).

Martin, A. E., & Gregg, R. D. (2017). Stable, Robust Hybrid Zero Dynamics Control of Powered Lower-Limb Prostheses. *IEEE transactions on automatic control, 62*(8), 3930-3942.

Martin, A. E., Post, D. C., & Schmiedeler, J. P. (2014). Design and Experimental Implementation of a Hybrid Zero Dynamics-Based Controller for Planar Bipeds with Curved Feet. *The International Journal of Robotics Research, 33*(7), 988-1005.

Martin, A. E., Villarreal, D. J., & Gregg, R. D. (2016). Characterizing and Modeling The Joint-Level Variability in Human Walking. *Journal of biomechanics, 49*(14), 3298-3305.

Martin, J., Pollock, A., & Hettinger, J. (2010). Microprocessor Lower Limb Prosthetics: Review of Current State of The Art. *JPO: Journal of Prosthetics and Orthotics, 22*(3), 183-193.

Marzen-Groller, K., & Bartman, K. (2005). Building A Successful Support Group for Post-Amputation Patients. *Journal of Vascular Nursing, 23*(2), 42-45.

McLaughlin, M. J. (2018). 10 - Lower Limb Amputation and Gait. In D. X. Cifu & H. L. Lew (Eds.), *Braddom's Rehabilitation Care: A Clinical Handbook* (pp. 57-65.e54): Elsevier.

Menezes Jr, J. M. P., & Barreto, G. A. (2008). Long-Term Time Series Prediction with The NARX Network: An Empirical Evaluation. *Neurocomputing, 71*(16-18), 3335-3343.

Miller, D. J., Stergiou, N., & Kurz, M. J. (2006). An Improved Surrogate Method for Detecting The Presence of Chaos in Gait. *Journal of biomechanics, 39*(15), 2873-2876.

Møller, M. F. (1993). A Scaled Conjugate Gradient Algorithm for Fast Supervised Learning. *Neural networks, 6*(4), 525-533.

Morantes, G., Cappelleto, J., Fernández, G., Clotet, R., Torrealba, R., & Guerrero, S. (2016). *Comparison of CPG Topologies for Bipedal Gait.* Paper presented at the 2016 IEEE Ecuador Technical Chapters Meeting (ETCM).

Moxey, P., Gogalniceanu, P., Hinchliffe, R., Loftus, I., Jones, K., Thompson, M., & Holt, P. (2011). Lower Extremity Amputations—A Review of Global Variability in Incidence. *Diabetic Medicine, 28*(10), 1144-1153.

Nandi, G. C., Ijspeert, A., & Nandi, A. (2008). *Biologically Inspired CPG Based Above Knee Active Prosthesis.* Paper presented at the 2008 IEEE/RSJ International Conference on Intelligent Robots and Systems.

Nesterov, Y. (1983). *A Method for Unconstrained Convex Minimization Problem with The Rate of Convergence O (1/k^ 2).* Paper presented at the Doklady an ussr.

Nocedal, J., & Wright, S. (2006). *Numerical Optimization*: Springer Science & Business Media.

Oliveira, P., & Pascoal, A. (1998). *Navigation Systems Design: An Application of Multi-Rate Filtering Theory.* Paper presented at the IEEE Oceanic Engineering Society. OCEANS'98. Conference Proceedings (Cat. No. 98CH36259).

Polak, E., & Ribiere, G. (1969). Note Sur la convergence de méthodes de directions conjuguées. *ESAIM: Mathematical Modelling and Numerical Analysis-Modélisation Mathématique et Analyse Numérique, 3*(R1), 35-43.

Prentice, S. D., Hasler, E. N., Groves, J. J., & Frank, J. S. (2004). Locomotor Adaptations for Changes in The Slope of The Walking Surface. *Gait & posture, 20*(3), 255-265.

Qian, N. (1999). On The Momentum Term in Gradient Descent Learning Algorithms. *Neural networks, 12*(1), 145-151.

Quintero, D., Martin, A. E., & Gregg, R. D. (2017). Toward Unified Control of a Powered Prosthetic Leg: A Simulation Study. *IEEE Transactions on Control Systems Technology, 26*(1), 305-312.

Rai, V., & Rombokas, E. (2019). *A Framework For Mode-Free Prosthetic Control For Unstructured Terrains.* Paper presented at the 2019 IEEE 16th International Conference on Rehabilitation Robotics (ICORR).

Rai, V., Sharma, A., & Rombokas, E. (2019). *Mode-free Control of Prosthetic Lower Limbs.* Paper presented at the 2019 International Symposium on Medical Robotics (ISMR).

Ramezani, A., Hurst, J. W., Akbari Hamed, K., & Grizzle, J. W. (2014). Performance Analysis and Feedback Control of ATRIAS, a Three-Dimensional Bipedal Robot. *Journal of Dynamic Systems, Measurement, and Control, 136*(2), 021012 (12 pages).

Reddi, S. J., Kale, S., & Kumar, S. (2019). On The Convergence of Adam and Beyond. *arXiv preprint arXiv:1904.09237*.

Robbins, H., & Monro, S. (1951). A Stochastic Approximation Method. *The Annals of Mathematical Statistics*, 22(3), 400-407.

Robitaille, B., Marcos, B., Veillette, M., & Payre, G. (1970). Quasi-Newton Methods for Training Neural Networks. *WIT Transactions on Information and Communication Technologies, 2*.

Roweis, S. (1996). Levenberg-Marquardt Optimization. *Notes, University Of Toronto*.

Ruder, S. (2016). An Overview of Gradient Descent Optimization Algorithms. *arXiv preprint arXiv:1609.04747*.

Scafetta, N., Marchi, D., & West, B. J. (2009). Understanding The Complexity of Human Gait Dynamics. *Chaos: An Interdisciplinary Journal of Nonlinear Science, 19*(2), 026108.

Shallue, C. J., Lee, J., Antognini, J., Sohl-Dickstein, J., Frostig, R., & Dahl, G. E. (2018). Measuring The Effects of Data Parallelism on Neural Network Training. *arXiv preprint arXiv:1811.03600*.

Shultz, A. H., Lawson, B. E., & Goldfarb, M. (2015). Variable Cadence Walking and Ground Adaptive Standing with a Powered Ankle Prosthesis. *IEEE transactions on neural systems and rehabilitation engineering, 24*(4), 495-505.

Simon, A. M., Ingraham, K. A., Fey, N. P., Finucane, S. B., Lipschutz, R. D., Young, A. J., & Hargrove, L. J. (2014). Configuring a Powered Knee and Ankle Prosthesis for Transfemoral Amputees within Five Specific Ambulation Modes. *PLoS ONE, 9*(6).

Spanias, J., Simon, A., Finucane, S., Perreault, E., & Hargrove, L. J. (2018). Online Adaptive Neural Control of a Robotic Lower Limb Prosthesis. *Journal of neural engineering, 15*(1), 016015.

Stepien, J. M., Cavenett, S., Taylor, L., & Crotty, M. (2007). Activity Levels Among Lower-Limb Amputees: Self-Report Versus Step Activity Monitor. *Archives of physical medicine and rehabilitation, 88*(7), 896-900.

Stolyarov, R., Burnett, G., & Herr, H. (2017). Translational Motion Tracking of Leg Joints for Enhanced Prediction of Walking Tasks. *IEEE Transactions on Biomedical Engineering, 65*(4), 763-769.

Sun, J., & Voglewede, P. A. (2014). Powered Transtibial Prosthetic Device Control System Design, Implementation, and Bench Testing. *Journal of Medical Devices, 8*(1).

Sup, F., Bohara, A., & Goldfarb, M. (2007). *Design and Control of A Powered Knee and Ankle Prosthesis.* Paper presented at the Proceedings 2007 IEEE International Conference on Robotics and Automation.

Sup, F., Varol, H. A., & Goldfarb, M. (2010). Upslope Walking with a Powered Knee and Ankle Prosthesis: Initial Results with an Amputee Subject. *IEEE transactions on neural systems and rehabilitation engineering, 19*(1), 71-78.

Sup, F., Varol, H. A., Mitchell, J., Withrow, T. J., & Goldfarb, M. (2009). Preliminary Evaluations of a Self-Contained Anthropomorphic Transfemoral Prosthesis. *IEEE/ASME Transactions on Mechatronics, 14*(6), 667-676.

Taga, G., Yamaguchi, Y., & Shimizu, H. (1991). Self-Organized Control of Bipedal Locomotion by Neural Oscillators in Unpredictable Environment. *Biological cybernetics, 65*(3), 147-159.

Tan, H. H., & Lim, K. H. (2019). *Review of Second-Order Optimization Techniques in Artificial Neural Networks Backpropagation.* Paper presented at the IOP Conference Series: Materials Science and Engineering.

Tian, Y., Wei, H., & Tan, J. (2012). An Adaptive-Gain Complementary Filter for Real-Time Human Motion Tracking With MARG Sensors in Free-Living Environments. *IEEE transactions on neural systems and rehabilitation engineering, 21*(2), 254-264.

Tlalolini, D., Chevallereau, C., & Aoustin, Y. (2010). Human-Like Walking: Optimal Motion of a Bipedal Robot With Toe-Rotation Motion. *IEEE/ASME Transactions on Mechatronics, 16*(2), 310-320.

Tucker, M. R., Olivier, J., Pagel, A., Bleuler, H., Bouri, M., Lambercy, O., Millán, J. d. R., Riener, R., Vallery, H., & Gassert, R. (2015). Control Strategies for Active Lower Extremity Prosthetics and Orthotics: a review. *Journal of NeuroEngineering and Rehabilitation*, 12(1), 1.

van den Berg, E. (2016). Some Insights into the Geometry and Training of Neural Networks. *arXiv preprint arXiv:1605.00329*.

Varol, H. A., Sup, F., & Goldfarb, M. (2008). *Real-Time Gait Mode Intent Recognition of A Powered Knee and Ankle Prosthesis for Standing and Walking.* Paper presented at the 2008 2nd IEEE RAS & EMBS International Conference on Biomedical Robotics and Biomechatronics.

Varol, H. A., Sup, F., & Goldfarb, M. (2009). Multiclass Real-Time Intent Recognition of a Powered Lower Limb Prosthesis. *IEEE Transactions on Biomedical Engineering, 57*(3), 542-551.

Wang, Q., Yuan, K., Zhu, J., & Wang, L. (2014). *Finite-State Control of A Robotic Transtibial Prosthesis with Motor-Driven Nonlinear Damping Behaviors for Level Ground Walking.* Paper presented at the 2014 IEEE 13th International Workshop on Advanced Motion Control (AMC).

Waters, R., Perry, J., Antonelli, D., & Hislop, H. (1976). Energy Cost of Walking of Amputees: The Influence of Level of Amputation. *J Bone Joint Surg Am, 58*(1), 42-46.

West, B. J., & Scafetta, N. (2003). Nonlinear Dynamical Model of Human Gait. *Physical review E, 67*(5), 051917.

Westervelt, E. R., Grizzle, J. W., Chevallereau, C., Choi, J. H., & Morris, B. (2018). *Feedback Control of Dynamic Bipedal Robot Locomotion*: CRC press.

Wilamowski, B. M. (2009). Neural Network Architectures and Learning Algorithms. *IEEE Industrial Electronics Magazine, 3*(4), 56-63.

Wilamowski, B. M., Yu, H., & Cotton, N. (2018). NBN Algorithm. In *Intelligent Systems* (pp. 13-11-13-24): CRC Press.

Yakovenko, S., Sobinov, A., & Gritsenko, V. (2018). Analytical CPG Model Driven by Limb Velocity Input Generates Accurate Temporal Locomotor Dynamics. *PeerJ, 6, e5849.*

Yao, Z., Gholami, A., Arfeen, D., Liaw, R., Gonzalez, J., Keutzer, K., & Mahoney, M. (2018). Large Batch Size Training of Neural Networks with Adversarial Training and Second-Order Information. *arXiv preprint arXiv:1810.01021*.

Young, A., Kuiken, T., & Hargrove, L. (2014). Analysis of Using EMG and Mechanical Sensors to Enhance Intent Recognition in Powered Lower Limb Prostheses. *Journal of neural engineering, 11*(5), 056021.

Young, A. J., & Hargrove, L. J. (2015). A Classification Method for User-Independent Intent Recognition for Transfemoral Amputees Using Powered Lower Limb Prostheses. *IEEE transactions on neural systems and rehabilitation engineering, 24*(2), 217-225.

Young, A. J., Simon, A. M., Fey, N. P., & Hargrove, L. J. (2014). Intent Recognition in a Powered Lower Limb Prosthesis Using Time History Information. *Annals of biomedical engineering, 42*(3), 631-641.

Young, A. J., Simon, A. M., & Hargrove, L. J. (2013). A Training Method for Locomotion Mode Prediction Using Powered Lower Limb Prostheses. *IEEE transactions on neural systems and rehabilitation engineering, 22*(3), 671-677.

Yuan, K., Wang, Q., & Wang, L. (2014). Fuzzy-Logic-Based Terrain Identification with Multisensor Fusion for Transtibial Amputees. *IEEE/ASME Transactions on Mechatronics, 20*(2), 618-630.

Zeiler, M. D. (2012). Adadelta: An Adaptive Learning Rate Method. *arXiv preprint arXiv:1212.5701*.

Zhang, F., DiSanto, W., Ren, J., Dou, Z., Yang, Q., & Huang, H. (2011). *A Novel CPS System for Evaluating A Neural-Machine Interface for Artificial Legs.* Paper presented at the 2011 IEEE/ACM Second International Conference on Cyber-Physical Systems.

Zhang, F., Dou, Z., Nunnery, M., & Huang, H. (2011). *Real-Time Implementation of An Intent Recognition System for Artificial Legs.* Paper presented at the 2011 Annual International Conference of the IEEE Engineering in Medicine and Biology Society.

Zhang, F., Liu, M., & Huang, H. (2012). *Preliminary Study of The Effect of User Intent Recognition Errors on Volitional Control of Powered Lower Limb Prostheses.* Paper presented at the 2012 Annual International Conference of the IEEE Engineering in Medicine and Biology Society.

Zhang, F., Liu, M., & Huang, H. (2014). Effects of Locomotion Mode Recognition Errors on Volitional Control of Powered Above-Knee Prostheses. *IEEE transactions on neural systems and rehabilitation engineering, 23*(1), 64-72.

Zhang, G. P. (2004). *Neural Networks in Business Forecasting*: IGI global.

Zheng, E., Wang, L., Wei, K., & Wang, Q. (2014). A Noncontact Capacitive Sensing System for Recognizing Locomotion Modes of Transtibial Amputees. *IEEE Transactions on Biomedical Engineering, 61*(12), 2911-2920.

List of Publications:

Al Kouzbary, H., Al Kouzbary, M., Tham, L. K., Liu, J., Shasmin, H. N., & Abu Osman, N. A. (2021). Generating an Adaptive and Robust Walking Pattern for a Prosthetic Ankle-Foot by Utilizing a Nonlinear Autoregressive Network With Exogenous Inputs. *IEEE Transactions on Neural Networks and Learning Systems*. (In Press)